Modeling of Circulation in the North Aleutian Basin

Department of the Interior, Bureau of Ocean Energy Management,

Regulation and Enforcement Program Number M07PC13368

Enrique N. Curchitser

Institute of Marine and Coastal Sciences, Rutgers University

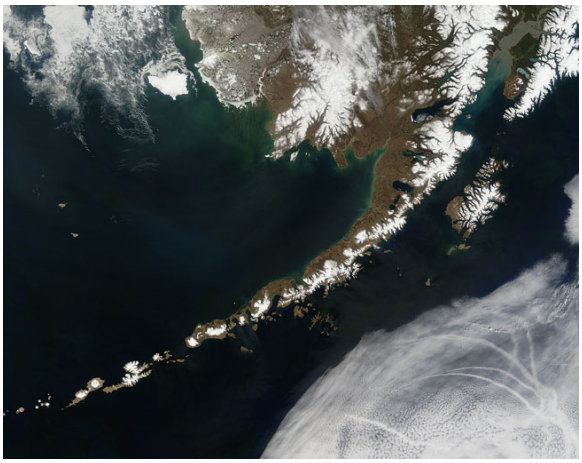

RUTGERS
Institute of Marine
and Coastal Sciences

Modeling of Circulation in the North Aleutian Basin

Department of the Interior, Bureau of Ocean Energy Management,

Regulation and Enforcement Program Number M07PC13368

Enrique N. Curchitser

Institute of Marine and Coastal Sciences, Rutgers University

71 Dudley Rd. New Brunswick, NJ 08901

Kate Hedstrom Seth Danielson Tom Weingartner

University of Alaska, Fairbanks

October, 2010

This study was funded by the U.S. Department of the Interior, Bureau of Ocean Energy Management, Regulation and Enforcement (BOEMRE), Alaska Outer Continental Shelf Region, Anchorage Alaska, under Contract No. M07PC13368, as part of the BOEMRE Environmental Studies Program.

Abstract

This document is a final report for the U.S. Department of Interior, Bureau of Ocean Energy Management, Regulation and Enforcement (BOEMRE) program M07PC13368, Modeling of Circulation in the North Aleutian Basin. The primary aim of the work done under this award was to use a state-of-the-art coupled circulation-sea ice numerical ocean model to simulate several decades of the currents in the North Aleutian Basin which can be used as inputs to oil-spill models. This document reviews the basic oceanography of the region of interest, describes the relevant details of the models and their implementation for this particular problem, and describes the extensive model-data comparisons that have been performed as part of the current award.

Contents

List of Figures

List of Tables

1 Introduction

1.1 Background: The Eastern Bering Sea

The physical oceanography of the eastern Bering Sea exhibits complex phenomena over a broad range of spatial and temporal scales, including tidal mixing, topographically steered flows, shelf-slope exchanges through canyons, mesoscale eddy mixing, flows through narrow passes and the yearly formation, drift, and melting of sea ice (Schumacher et al. 2003).

A description of the current systems in the Bering Sea, schematically illustrated in Figure 1, can be found in Stabeno et al. (1999). Inflow to the Bering Sea occurs through the Aleutian Passes, predominantly Amukta and Amchitka Passes and Near Strait. The principle outflow is through Kamchatka Strait to the west. While transport through the Bering Strait is small (0.8 Sv; Roach et al. 1995), the flow from the Bering to the Arctic strongly dominates the flow patterns of the northern Bering Sea shelf.

The eastern Bering Sea has the following primary physical features: 1. *Principal Currents:* The principal currents in the eastern Bering Sea basin are the Aleutian North Slope Current (ANSC, Stabeno and Reed 1994; Stabeno et al. 1999) and the Bering Slope Current (BSC; Schumacher and Reed 1992). The ANSC flows along the northern side of the Aleutian Islands. The source of these waters is predominately through Amchitka and Amukta Pass. The ANSC is the source of the BSC, which is the eastern boundary current of the cyclonic circulation of the Bering Sea basin (Stabeno and Reed 1994). 2. *Tidal influence:* The eastern Bering Sea (EBS) is strongly influenced by tidal mixing, as well as subtidal flows driven by wind and buoyancy. Subtidal flows interact with tides through the density field. The intense tidal and wind mixing, coupled with stratification by solar heating, leads to three domains

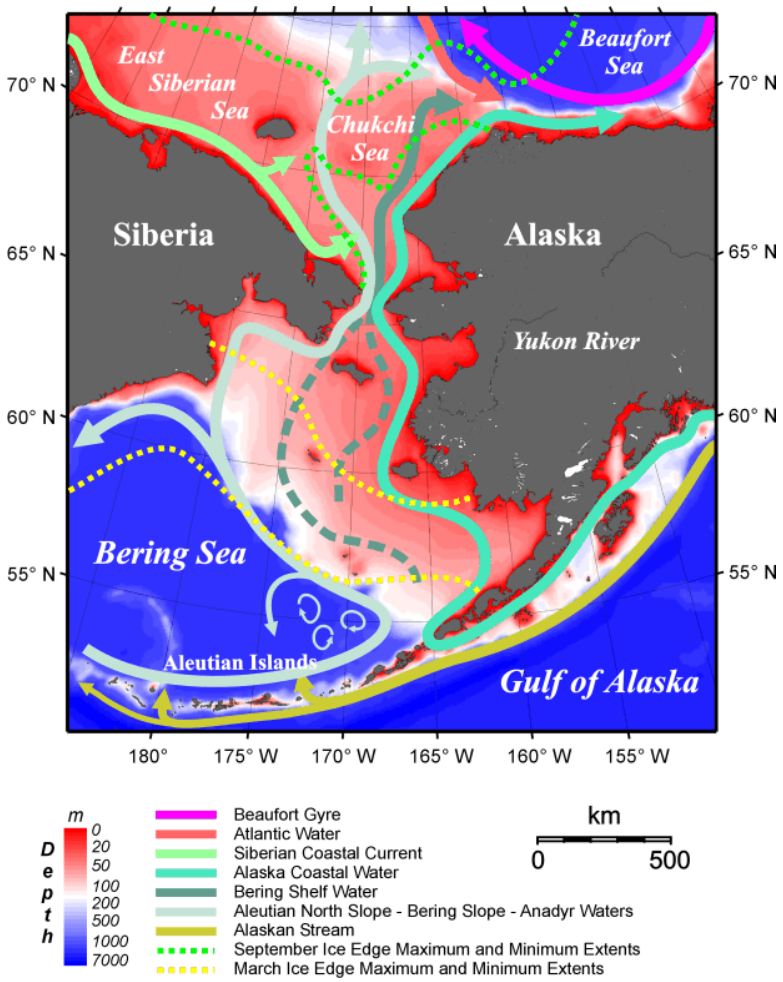

Figure 1: Schematic of the circulation in the Bering Sea

on the shelf (Coachman 1986; Coachman 1982; Schumacher and Stabeno 1998). The coastal domain (0-50 m bottom depth) is well mixed or weakly stratified. The middle domain (50-100 m) is characterized by a two-layer system. The outer domain ($> 100m$), more oceanic in character, exhibits mixed layers at the surface and bottom with a stratified layer between. The importance of including both tidal and subtidal flows in numerical simulations of the southeastern Bering Sea shelf was shown in Hermann et al., (2002). 3. *Shelf-slope exchange:* Exchange between shelf and slope waters provides for a vigorous tracer exchange but the magnitude of this exchange is not well measured. Flow onto the shelf is a combination of currents interacting with topography (e.g. canyons) and instabilities of shelf break flows (Stabeno and Van Meurs 1999). 4. Meanders and eddies: Meanders and eddies are common over the southeast corner of the basin (Schumacher and Stabeno 1994). Altimetric, SST and drifter data have revealed mesoscale features on 20-200 km scales. 5. Ice physics and the cold pool: Ice forms in the the northern Bering Sea during winter. This sea ice is advected south into the SEBS, where the leading edge melts. This is one of the main mechanisms contributing to the heat and salt content and density stratification and vertical mixing of shelf waters. A persistent pool of cold water ($< 2^oC$) forms over the northern shelf each year and over the southern shelf in years of extensive ice cover. Fresh water from melting ice plays an important role in the spring setup of the 2-layer system (Stabeno et al. 2001).

2 Scientific and technical approaches

2.1 The coupled ocean-sea ice model

The main research tool used for this work is a state-of-the-art coupled ocean/sea ice model based on the Regional Ocean Modeling System (ROMS). ROMS is a free-surface, hydrostatic primitive equation ocean circulation model whose core was developed at Rutgers University and UCLA with significant contributions from a large community of users. ROMS is a terrain-following, finite difference (Arakawa C-grid) model with the following advanced features: extensive restructuring for sustained performance on multi-processor computing platforms (using MPI); high-order, weakly dissipative algorithms for tracer advection; a unified treatment of surface and bottom boundary layers (e.g., K-Profile Parameterization; Large et al., 2004), atmosphere-ocean flux computations based on the ocean model prognostic variables using bulk-formulae (Fairall et al., 1996) and an integrated set of procedures for data assimilation (e.g., optimal interpolation and adjoint-based methods; Moore et al., 2004). ROMS also has an integrated float tracking capability. The vertical discretization is based on a terrain-following coordinate system with the ability to increase the resolution near the surface and bottom boundary layers.

ROMS has been coupled to a sea-ice model (Budgell, 2005) consisting of the elastic-viscous-plastic (EVP) rheology (Hunke and Dukowicz, 1997) and the Mellor and Kantha (1989) thermodynamics. It is fully explicit and implemented on the ROMS Arakawa C-grid and is therefore fully parallel using MPI, just as ROMS is. The model also includes frazil ice growth in the ocean being passed to the ice (Steele et al., 1989). It currently follows a single ice category, which exhibits accurate results in a marginal ice zone such as the Bering Sea.

The principal attributes of the model are:

1. General
   (a) Primitive equations with potential temperature, salinity, and an equation of state.
   (b) Hydrostatic and Boussinesq approximations.
   (c) Optional third-order upwind advection scheme.
   (d) Optional Smolarkiewicz advection scheme for tracers (potential temperature, salinity, etc.).
   (e) Optional Lagrangian oats.
   (f) Option for point sources and sinks.
2. Horizontal
   (a) Orthogonal-curvilinear coordinates.
   (b) Arakawa C grid.
   (c) Closed basin, periodic, prescribed, radiation, and gradient open boundary conditions.
   (d) Masking of land areas.
3. Vertical
   (a) sigma (terrain-following) coordinate.
   (b) Free surface.
   (c) Tridiagonal solver with implicit treatment of vertical viscosity and diffusivity.

4. Ice

   (a) Hunke and Dukowicz elastic-viscous-plastic dynamics.

   (b) Mellor-Kantha thermodynamics.

   (c) Orthogonal-curvilinear coordinates.

   (d) Arakawa C grid.

   (e) Smolarkiewicz advection of tracers.

5. Mixing options

   (a) Horizontal Laplacian and biharmonic diffusion along constant s, z or density surfaces.

   (b) Horizontal Laplacian and biharmonic viscosity along constant s or z surfaces.

   (c) Optional Smagorinsky horizontal viscosity and diffusion (but not recommended for diffusion).

   (d) Horizontal free-slip or no-slip boundaries.

   (e) Vertical harmonic viscosity and diffusion with a spatially variable coefficient, with options to compute the coefficients with Large et al., Mellor-Yamada, or generic length scale (GLS) mixing schemes.

6. Implementation

   (a) Dimensional in meter, kilogram, second (MKS) units.

   (b) Fortran 90.

   (c) Runs under UNIX, requires the C preprocessor, gnu make, and Perl.

(d) All input and output is done in NetCDF (Network Common Data Format), requires the NetCDF library.

(e) Options include serial, parallel with MPI, and parallel with OpenMP.

Exhaustive details of the model are provided in the accompanying manual which is part of the deliverables for this contract (Hestrom, 2010, MMS 2009-062).

2.2 Bering Sea Implementation

Figure 2 shows the set of nested model domains currently implemented in the north Pacific ocean, ranging from 4 km in the Bering Sea (BERING) to 10 km in the Northeast Pacific (NEP) to 0.18 deg North Pacific (NPac) grids. Since the current contract called for a multi-decadal integration, we settled for the 10 km horizontal resolution NEP domain (domain 2 in figure 2). This domain captures the circulation both in the Bering Sea and the Gulf of Alaska which is crucial to the physics of the North Aleutian Basin and is easily affordable for the required timescales.

The NEP model extends from approximately 20 N to 71 N. It extends about 2250 km offshore from the North America west coast at a nominal horizontal resolution of 10 km and 60 terrain-following vertical levels stretched towards the surface boundary. The terrain-following coordinate system has distinct advantages for modeling shelf regions; The full vertical coordinate system is compressed over the shelf resulting in high vertical resolution in the region of interest (e.g., 60 layers over the whole Bering Sea shelf in the current NEP implementation) and as a consequence no computations are wasted in the bathymetry. The grid (a rectangle in a Lambert Conical projection) is rotated relative to lines of constant

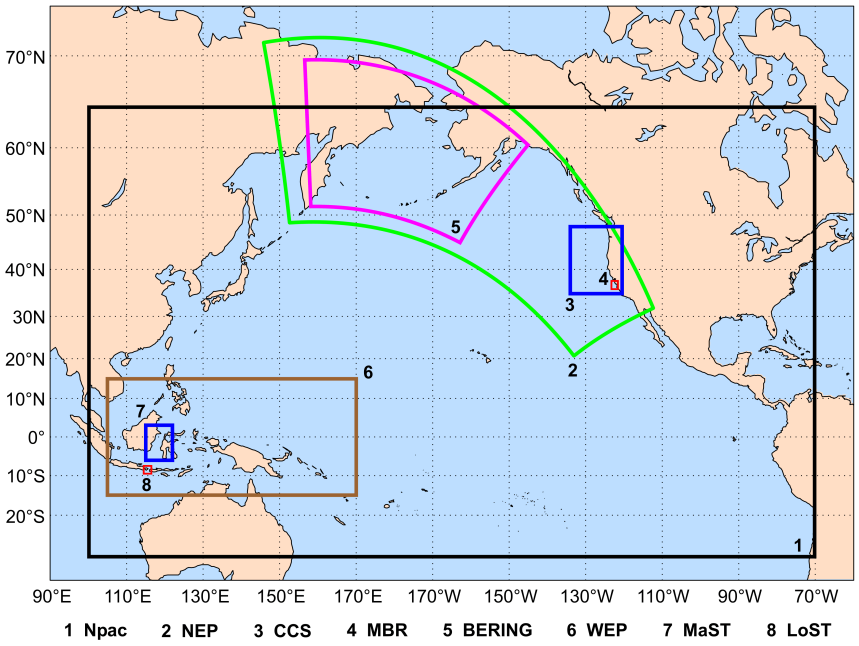

Figure 2: A suite of nested models in the North Pacific. The models relevant to the Bering Sea are (1) The North Pacific (NPac 0.18 deg.), (2) The Northeast Pacfic (NEP at 10 km) and (5) BERING, currently

longitude so as to minimize computations over land. The coupled ocean/sea ice model has been integrated for the period of 1958 through 2004. The surface forcing for the NEP model is derived from the datasets for Common Ocean-ice Reference Experiments version 2 (CORE v2; Large and Yeager, 2004), which consists of 6-hourly winds, air temperatures, sea level pressure and specific humidity, daily short-wave and downwelling long-wave radiation, and monthly precipitation. The air-sea fluxes are computed using bulk formulae (Fairall et al., 1996). The oceanic surface boundary layer is computed using the k-profile parameterization (Large et al., 1994). Riverine inputs are implemented as a surface fresh water flux which guarantees global conservation over long-timescales. Boundary and initial conditions for this domain were derived from the Simple Ocean Data Assimilation (SODA 2.0.2; Carton et al., 2000a,b) which is an ocean reanalysis product for the 1958-2006 period. The nominal resolution of SODA is 0.5 degrees and we were able to obtain 5-day averages for the boundary conditions. The northern boundary has a sink term which is set to enforce a 0.8 Sv northward transport through the Bering Strait.

Tidal forcing is implemented through the boundaries using the eight dominant diurnal and semi-diurnal components derived from the Oregon State Tidal Prediction Software (Egbert and Erofeeva, 2001) (OTPS;
http://www.coas.oregonstate.edu/research/po/research/tide/global.html).

One significant aspect to simulating tides well is a good representation of the bathymetry. To that end, we used a newly available Alaska region bathymetric dataset that was constructed solely from observational soundings (figure 3) blended with a conventional ETOPO dataset for the regions south of 45N. The resulting model bathymetry is shown in figure 4.

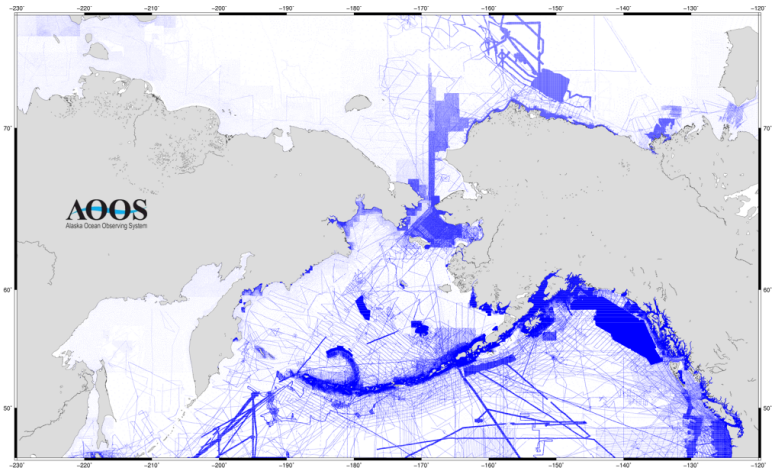

Figure 3: Soundings used to generate custom bathymetry for the Bering Sea and Gulf of Alaska.

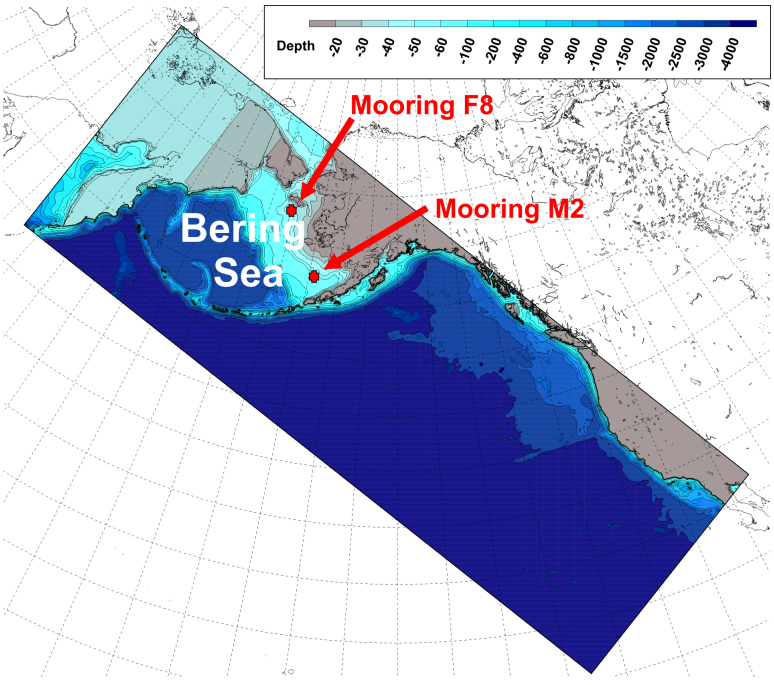

Figure 4: Model domain in native projection and resulting bathymetry.

3 Model-data comparisons

An integral part of this project is model skill assessment. We will rely on historical observational datasets for model validation. Although not all of the datasets are located strictly within the North Aleutian Basin (NAB) domain, model-data comparisons in the NAB and on the greater Bering Sea shelf will provide the most robust evaluations of model performance in both regions. We first describe the data that we have selected for comparisons and then show results.

3.1 Datasets

Oceanographic mooring data from two primary sites are used to evaluate the bulk statistical properties of the temperature, salinity and current fields (Figure 4). The comparisons include evaluation of interannual, seasonal , synoptic and tidal variability. Multi-year time series are available from the NOAA site M2 within the NAB (1995-present, 56 36.20' N; 164 38.00' W; P. Stabeno, unpubl. data). We also use data from a mooring (F8) deployed just south of St. Lawrence Island from September 1998 to September 1999. The M2 mooring has temperature and salinity measurements at various depths and a profiling current meter. M2 is used to assess both the local stratification and currents in the model. The F8 mooring data is used to assess the vertical structure of tidal currents. Mean current speed and direction from mooring data in the published literature base are used to make point comparisons of velocity to modeled currents. Other datasets used are SSM/I satellite data for ice cover, drifter data for surface velocity comparisons, CTD hydrographic samples from the UAF-IMS and the NODC-WOD databases, and tidal elevation stations throughout the Bering Sea.

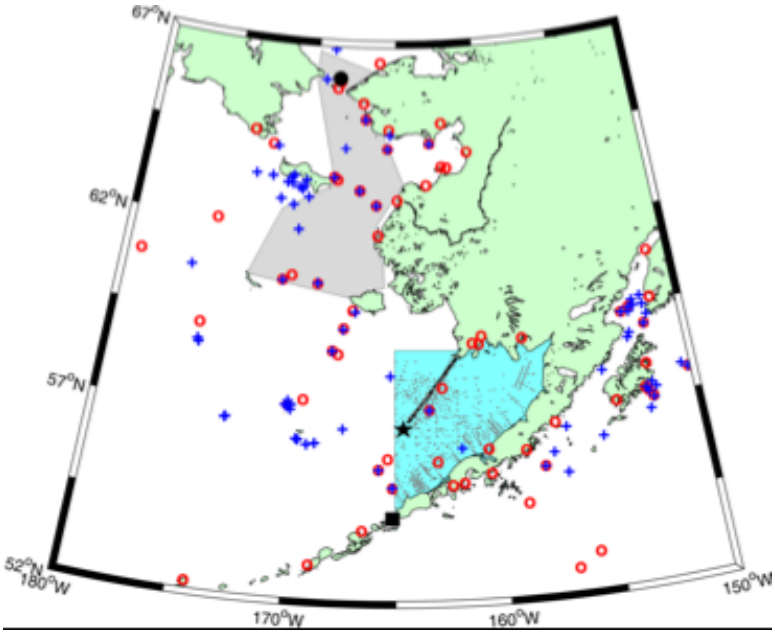

Figure 5: Map showing the location of observational data available for model comparisons. The NAB planning area is shaded light blue. Small grey dots within the NAB indicate CTD hydrographic samples locations from the UAF-IMS and the NODC-WOD databases. Samples along the Cape Newenham to M2 transect (thick black line) will form the primary section for hydrographic comparisons of fronts and stratification locations and strengths. Multi-year temperature, salinity and current measurements are made on moorings at site M2 (star), Bering Strait (black solid circle) and Unimak Pass (black solid square). Red open circles denote tidal elevation harmonics stations and blue plus signs denote tidal current ellipse harmonics stations. The light purple shaded area indicates the approximate domain of the 2002 surface drifter tracks.

3.2 Model Evaluation

The following are the model evaluation metrics that are being carried out as part of this project:

1. Tidal heights and currents
    (a) Amplitudes and Phases
    (b) Current ellipse parameters
    (c) Vertical tidal current structure
2. Sub-tidal currents
    (a) Spectral comparisons
    (b) Mean flow comparisons
3. T and S variability
    (a) Monthly means and anomalies over the shelf at mooring M2
    (b) Across the NAB, the whole Bering shelf and the Bering basin
4. Density gradients
    (a) Cross-isobath structure
    (b) Frontal locations
    (c) Frontal strength
    (d) Vertical density gradients: magnitude and location within water column

5. Ice cover

   (a) Spatial/point time series

   (b) EOFs

We now proceed to present some of these comparisons:

3.2.1 Tides

The cotidal maps (Figure 6) are compared to those of Kowalik [1999]. The overall pattern of the co-phase lines is very similar and typically within 15-30 in the deep basins. Amphridromic points in the Gulf of Anadyr, Norton Sound, near St. Lawrence Island, near Nunivak Island and near Cape Newenham are reproduced. Co-amplitudes lines also exhibit similar patterns and magnitudes.

Examination of the tidal ellipse parameters for the M2 and K1 constituents (Figures 7-11) shows that the model captures the basic behavior of the tidal bottom boundary layer (BBL) effects. These include the following. 1) The semidiurnal (M2) BBL extends farther from the seafloor than the diurnal (K1) BBL. 2) Stratification effects appear to impact the M2 BBL, resulting in enhanced M2 currents during the late summer and early fall when the vertical density gradient is at its annual maximum. M2 tidal current can exhibit a subsurface maximum.

The M2 amplitude comparison presented in Figure 12 (top left panel), shows that on average the model slightly overestimates the observed M2 elevations although the slope of the fit is close to 1:1. The elevation phases (lower left panel) shows an offset of approximately 60 degrees for many stations and scatter on the order of another 60 degrees. The closely

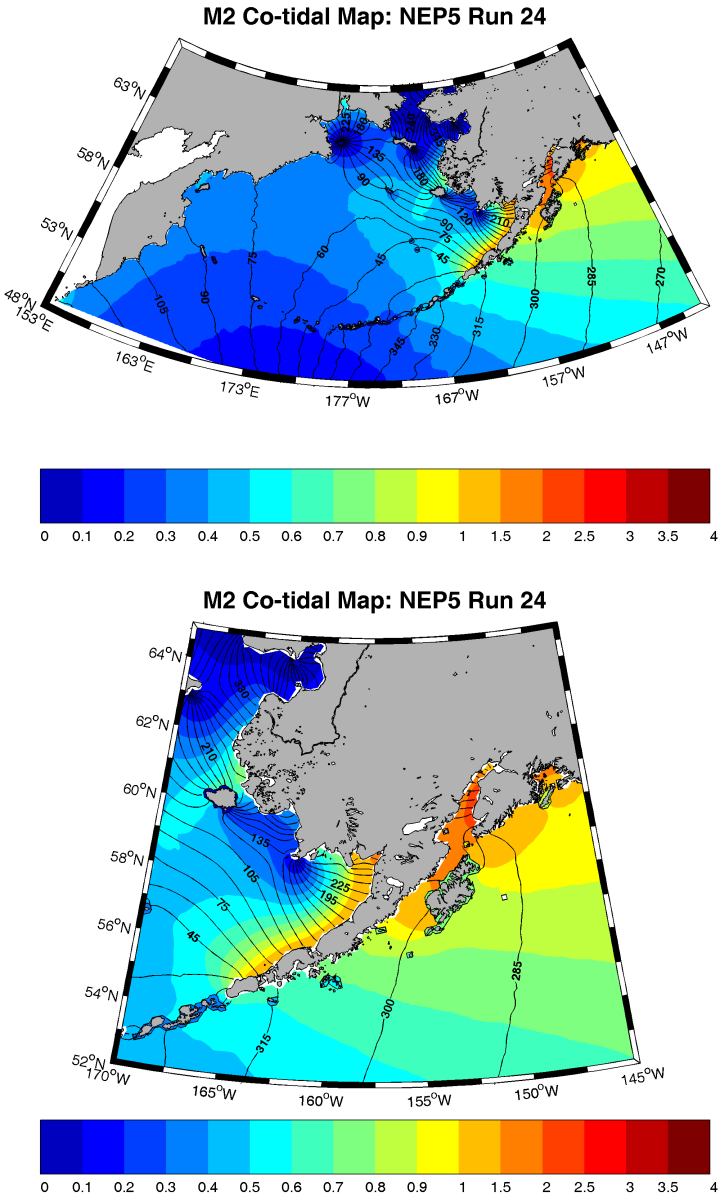

Figure 6: Model co-tidal map for the Bering Sea (top) and a zoom of the southeastern Bering region (bottom).

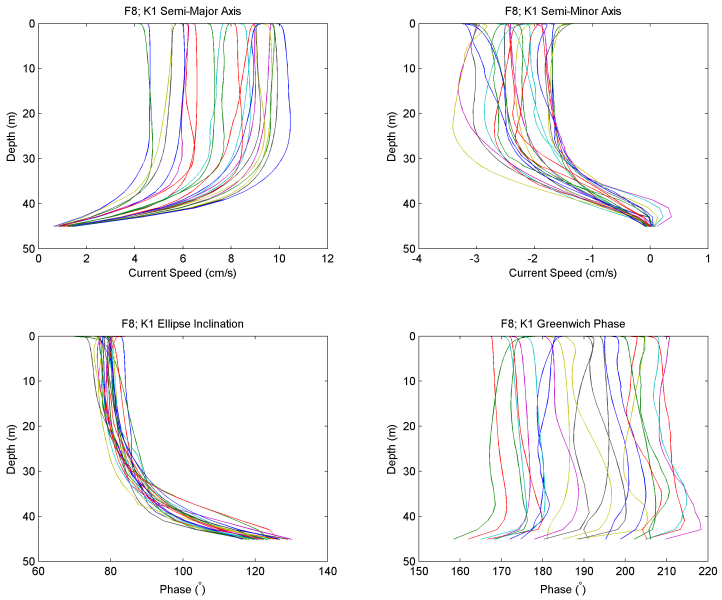

Figure 7: Depth profiles for K1 tidal component.

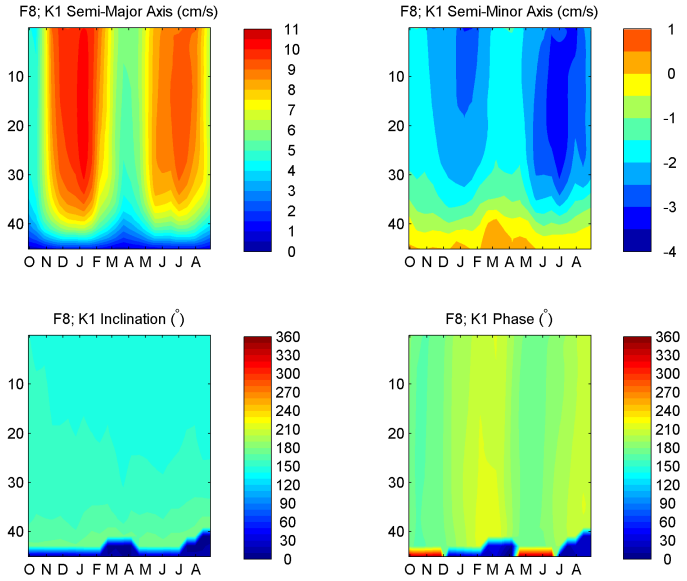

Figure 8: Time evolution of K1 tidal component

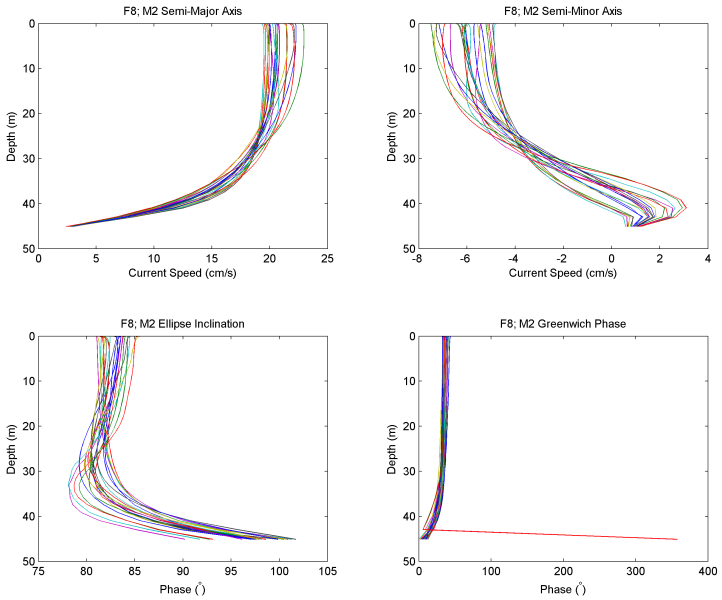

Figure 9: Depth profiles for M2 tidal component.

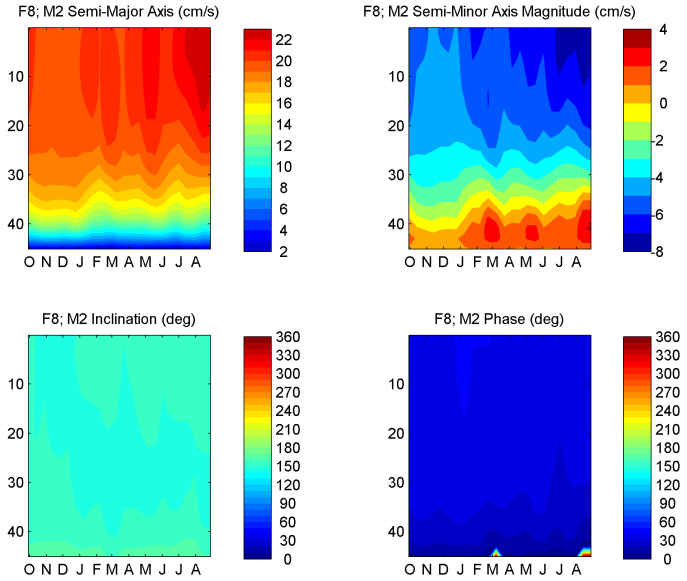

Figure 10: Time evolution of M2 tidal component

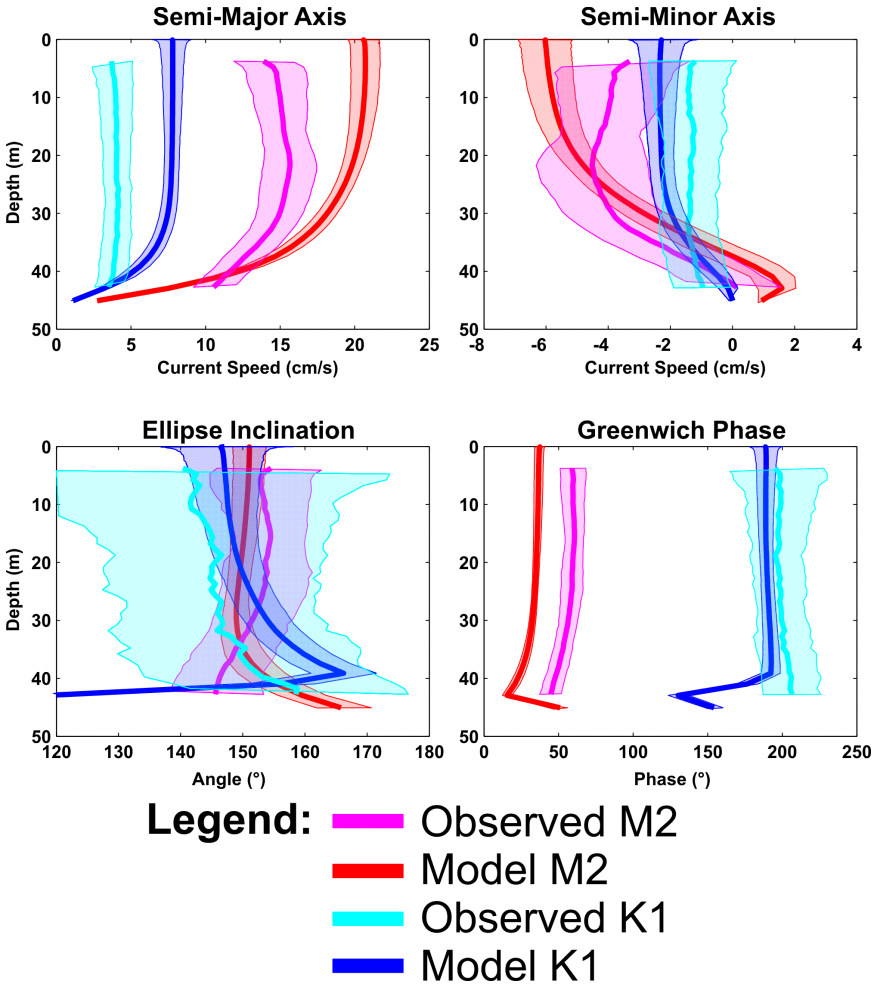

Figure 11: Mean profiles for M2 and K1 tidal components

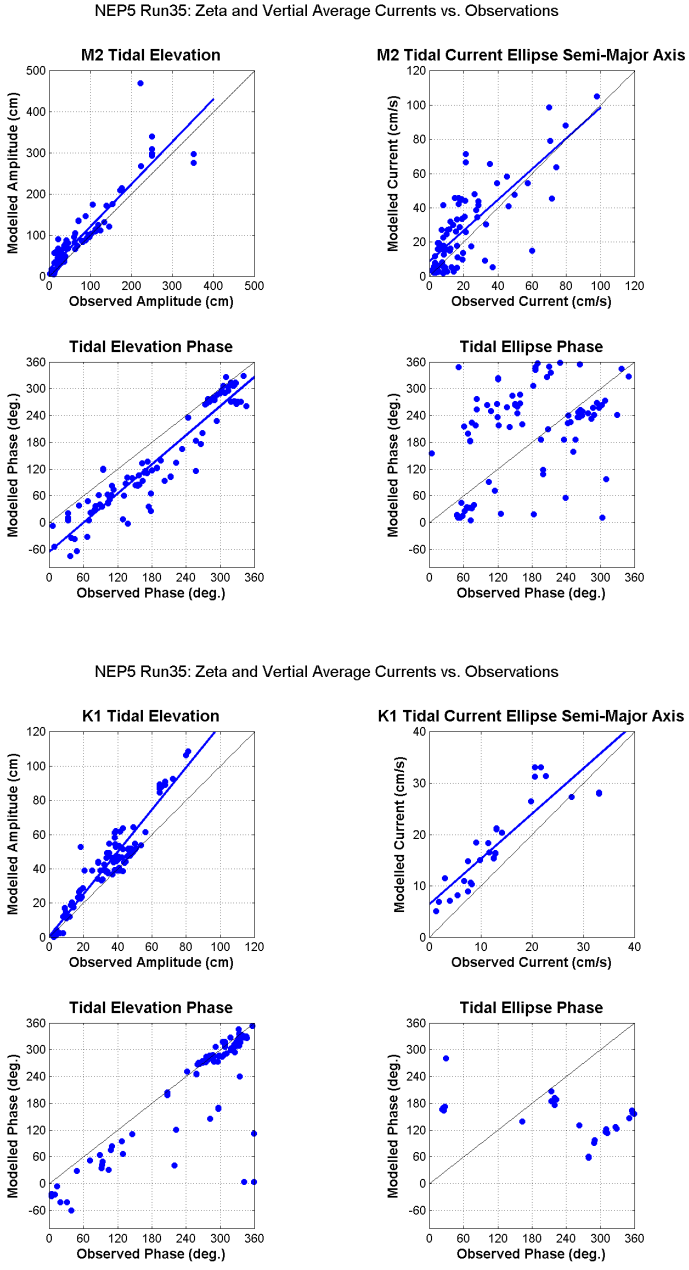

Figure 12: Model versus observations scatter plots of elevation amplitude and phase and ellipse phases for the M2 (top) and K1 (bottom) tidal components.

clustered stations that lie on the 1:1 line between 240 and 360 degrees are comprised of stations that are found mostly in deep waters in the northern and western Gulf of Alaska. This shows that the tidal phasing is correct as it propagates northward and that the tidal elevation wave is retarded in the model with respect to the observations. It is likely that this phase change occurs as the tidal wave crosses the Aleutian Island chain or when it impinges upon the shelf.

Because the velocity field is closely tied to the sea surface elevation slope, it is often more difficult to simulate. The M2 currents show more relative scatter than the amplitudes but the fit also closely follows the 1:1 line. Phasing of the tidal ellipses are also nearly 60 degrees offset from that observed. Note that within tidal ellipses, there can exist an ambiguity of 180 degrees so the scatter shown in the lower right panel over-emphasizes the actual scatter.

3.2.2 Velocities

Because of a lag in obtaining forcing data, the model was not run for 2008 and 2009 - when most of our drifter data was collected - so we make seasonally averaged comparisons rather than direct time-matched comparisons. These are presented in figures 13-21. The drifter data suggest a seasonal reorganization of the surface currents, with the nearshore region exhibiting mostly along-shore motion during the summer accompanied by little offshore spreading. In the fall and winter months, the drifters show a pronounced westward motion. These two behaviors appear to be captured by the model.

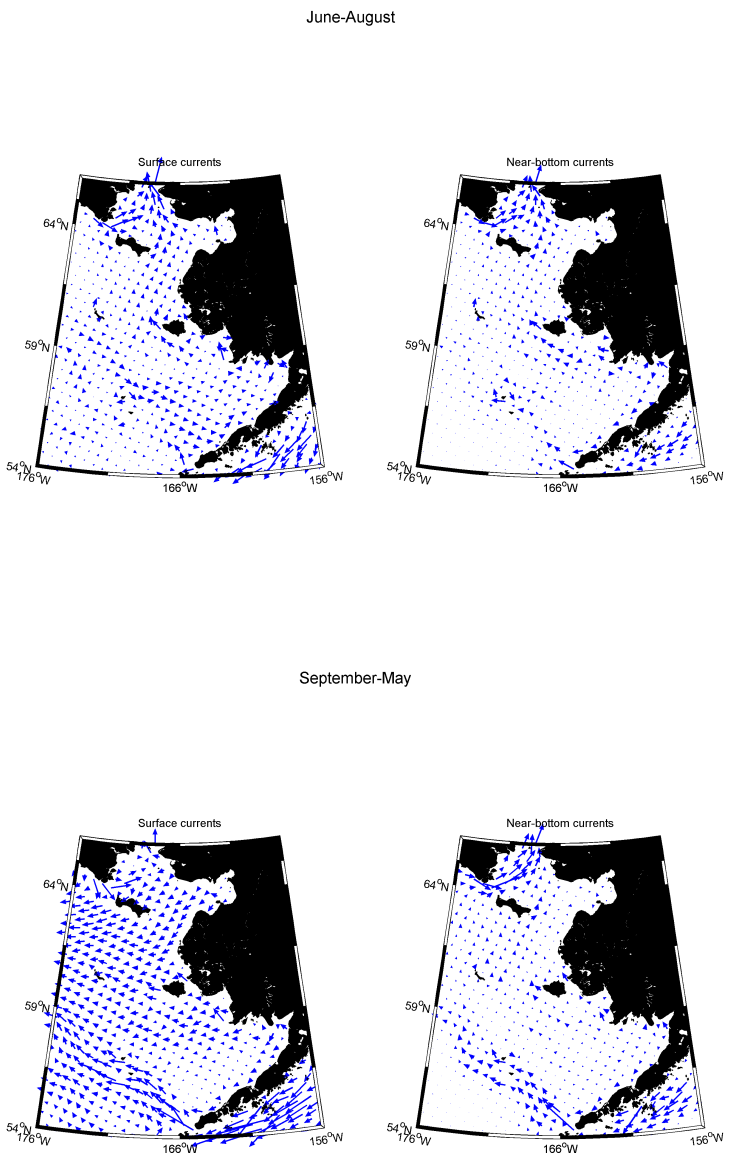

Figure 13: Seasonal surface and bottom currents.

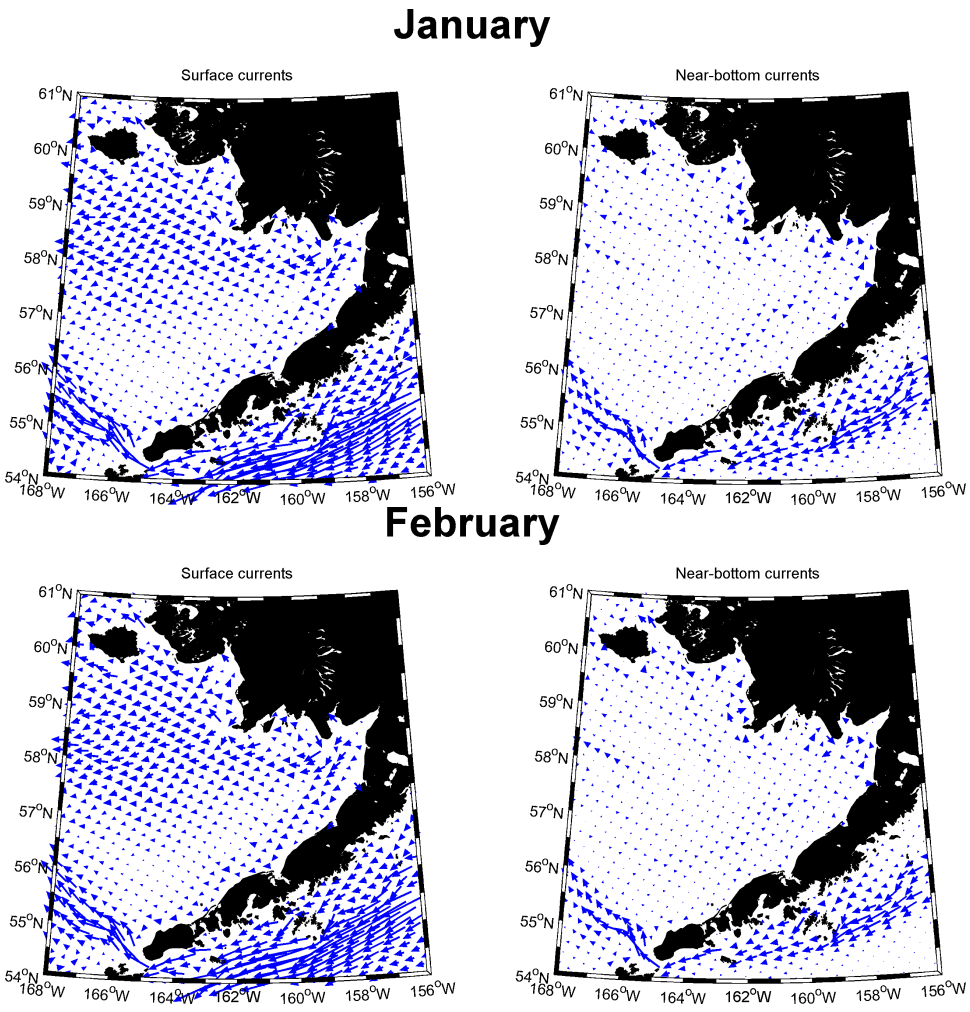

Figure 14: Monthly averaged surface and bottom currents (January and February).

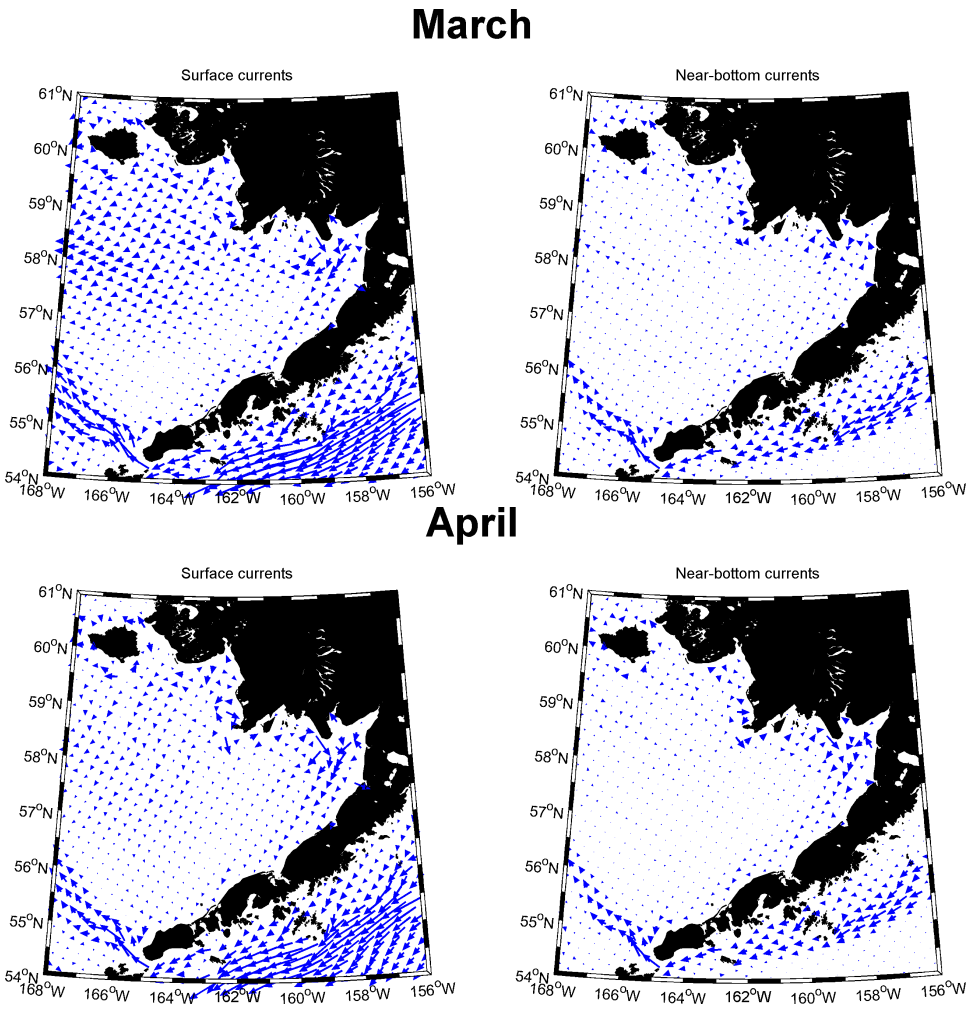

Figure 15: Monthly averaged surface and bottom currents (March and April).

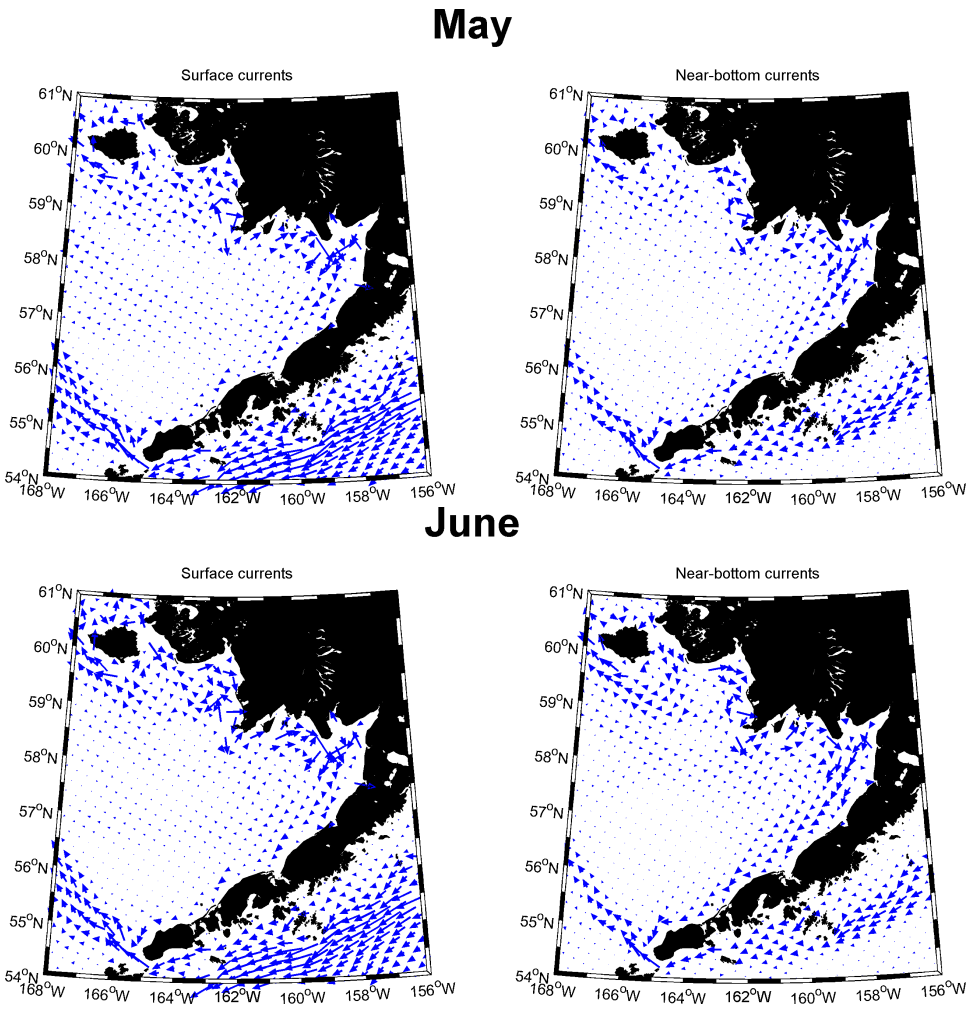

Figure 16: Monthly averaged surface and bottom currents (May and June).

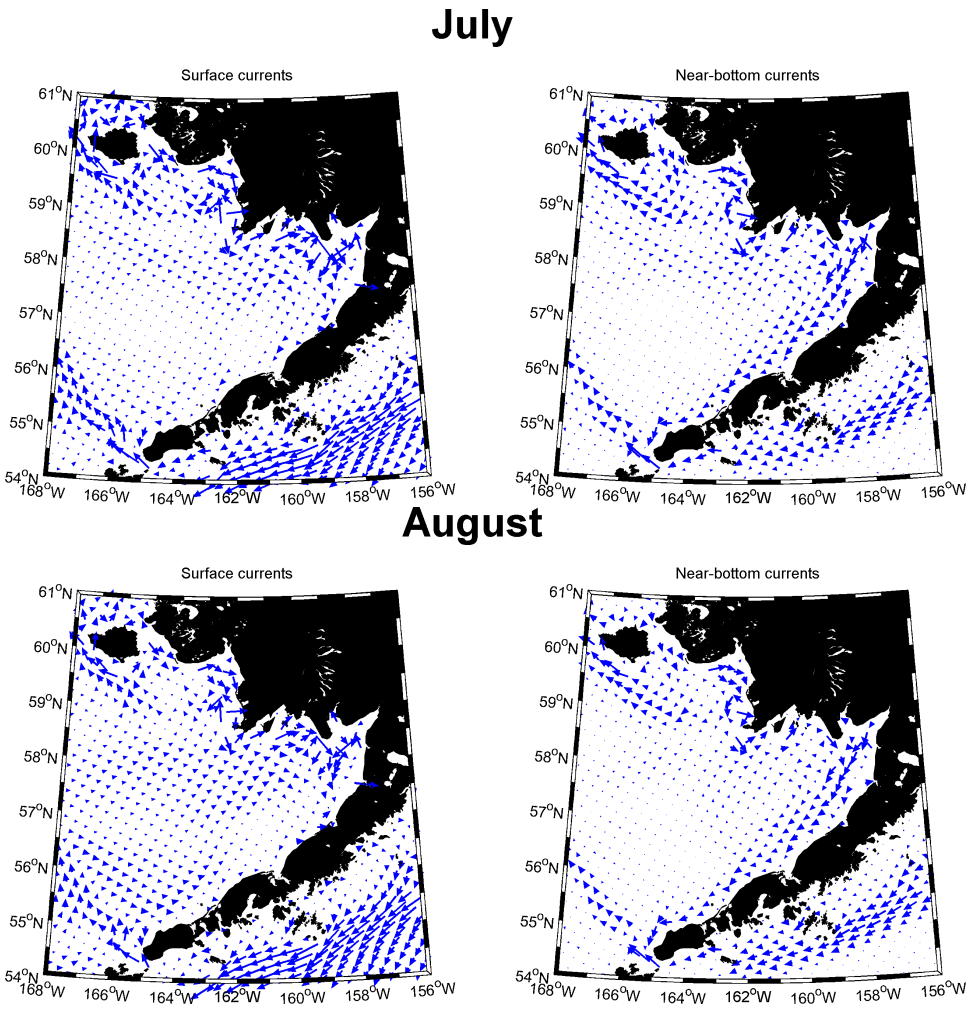

Figure 17: Monthly averaged surface and bottom currents (July and August).

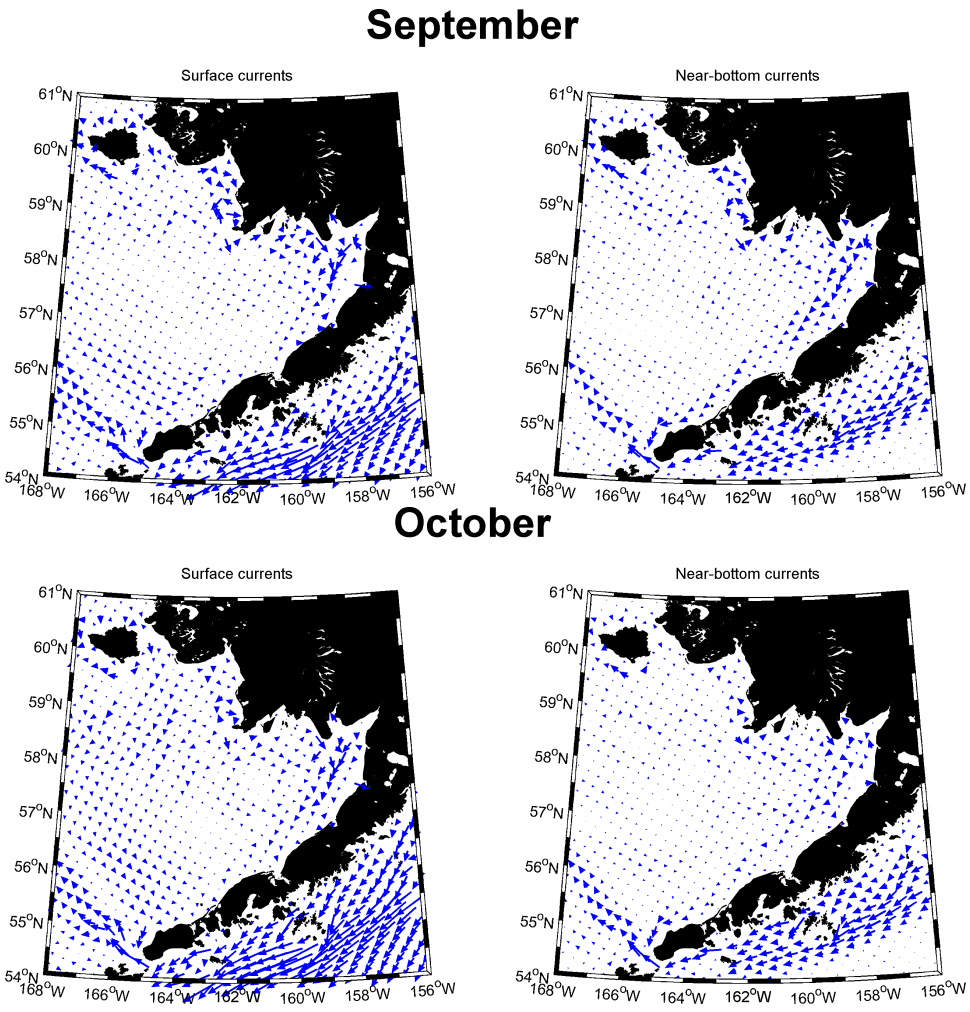

Figure 18: Monthly averaged surface and bottom currents (September and October).

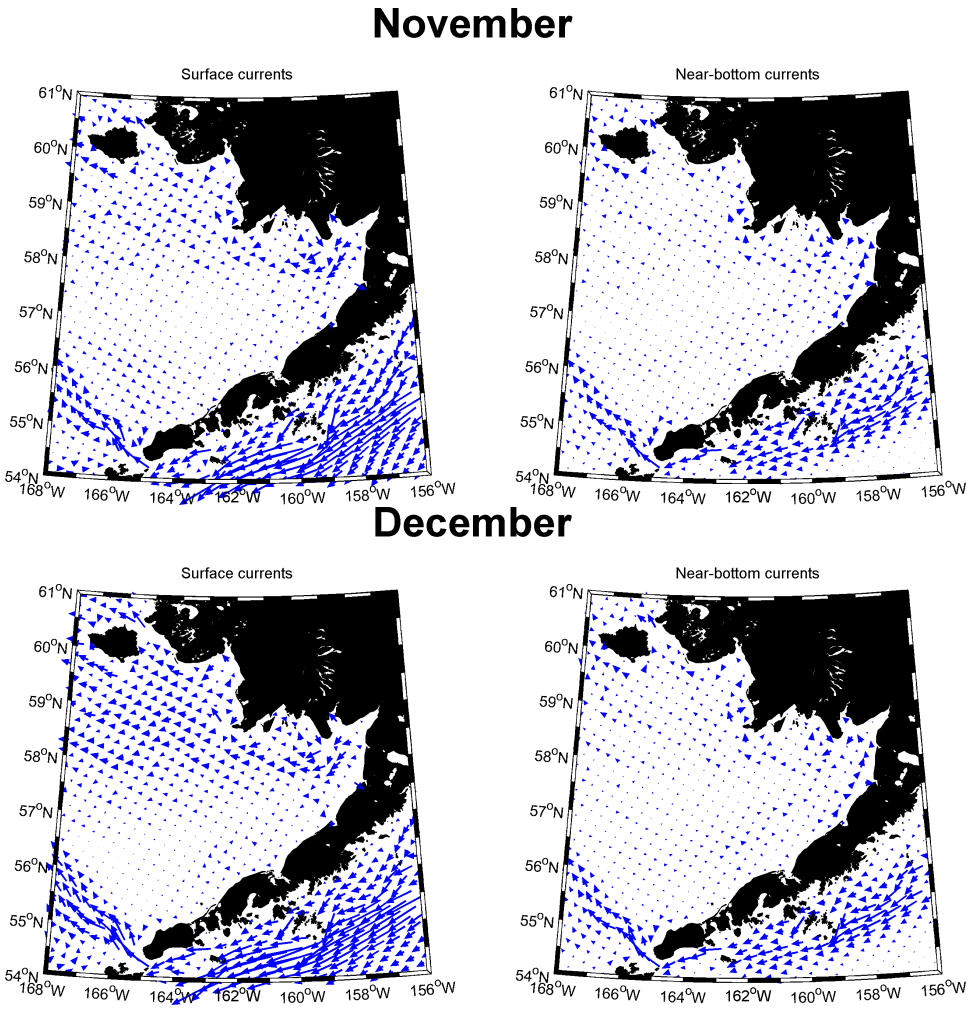

Figure 19: Monthly averaged surface and bottom currents (November and December).

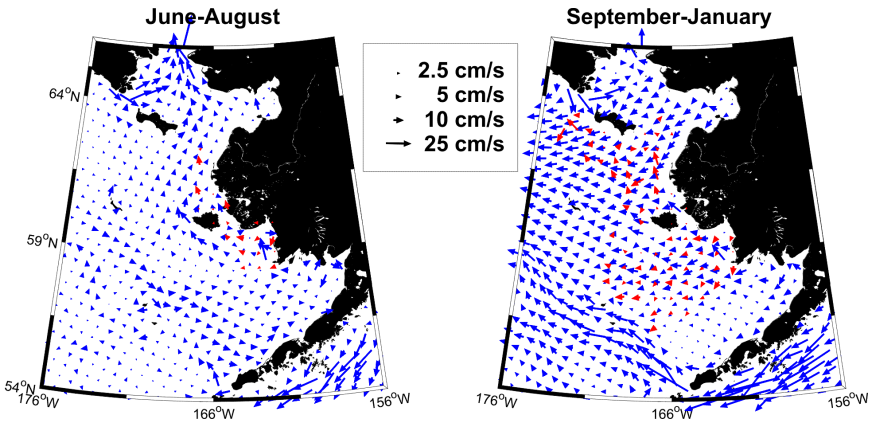

Figure 20: Comparison of model (blue) and drifter (red) velocities.

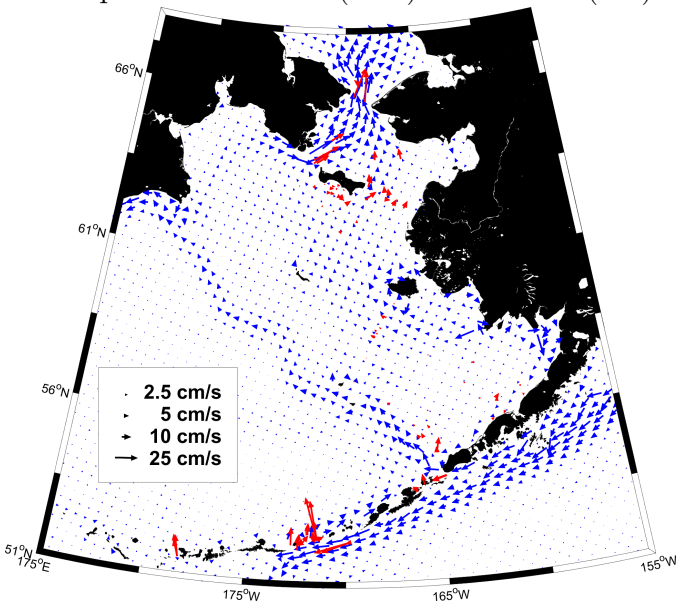

Figure 21: Comparison of model (blue) and drifter (red) velocities.

3.2.3 Sea-ice

Figure 22 (top), presents the model and satellite-derived ice extent for all the years of the model run. The model clearly shows skill in reproducing both the magnitude and interanual variability in this field. The bottom of the figure is the model derived ice thickness, for which there is no significant time series available in the Bering sea.

The following figures (23-26) present spatial maps of the sea ice fields. The blue contours (Figure 23) show the mean monthly observed ice concentrations (10% concentration contour interval). The colors show the difference between the model and the observation, with differences contoured at the 10% concentration level. Warm (red) colors indicate the model concentration is greater than those observed; cool (blue) colors indicate the model concentrations are less than those observed. We find that the model is typically within 10-20% of that observed, underestimating the ice concentrations in and south of the Gulf of Anadyr in the mid to late winter and overestimating concentration in the late spring/early summer in the northern central region.

The blue contours in Figure 24 show the monthly mean observed ice concentrations (10% concentration contour interval). The RMSE is typically between 10 and 30%. The largest errors appear in the western Gulf of Anadyr during the spring and early summer months.

In Figure 25, the color contours show the difference, in standard deviation between the model and the observations. Differences in standard deviation are typically less than +/- 20%. Ice variation is typically greater in the observed fields in the mid and late winter whereas the model shows slightly greater variation in the late spring and early summer.

In Figure 26, the blue contours show the mean monthly observed ice concentrations

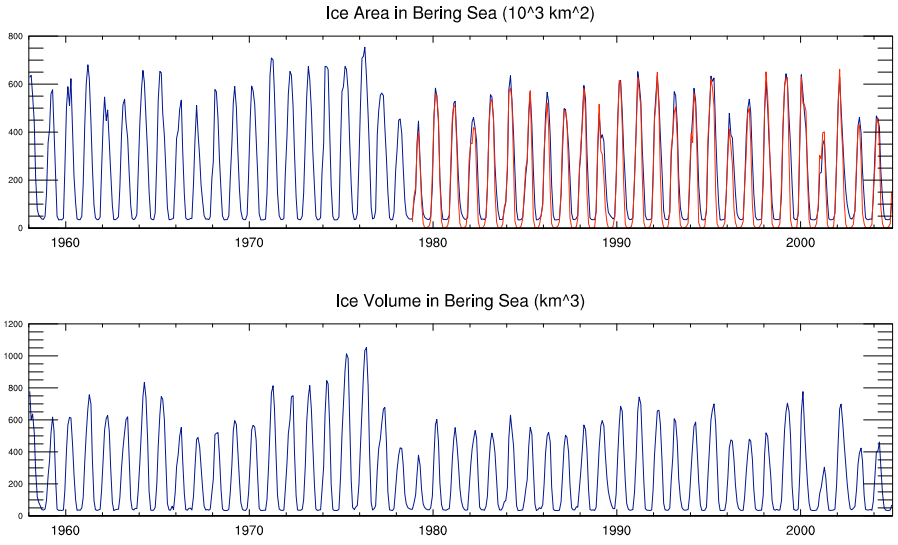

Figure 22: Time series of bulk sea ice area (top) and volume (bottom). Blue is model, red SSM/I satelite data, when available.

(10% concentration contour interval). Yellow contours denote the region that is significant at the 95% confidence interval. We find that extensive regions beyond the low mean ice concentration of 10% are significantly correlated, which indicates that years of extensive ice are well captured by the model. The Gulf of Anadyr, Anadyr Strait and Chirikov Basin regions have the most consistently non-correlated grid points. This may be due to the boundary conditions forcing flow through the Bering Strait rather than a result of model dynamics. Because the northward transport through Bering Strait is prescribed, the flow field in Anadyr Strait is not tightly coupled to the regional wind field, which has been shown to strongly impact the instantaneous transport through Bering Strait. Shpanberg Strait is not impacted to the same degree because a much greater proportion of the Bering Strait throughflow comes from the western side of St. Lawrence Island rather than the eastern side.

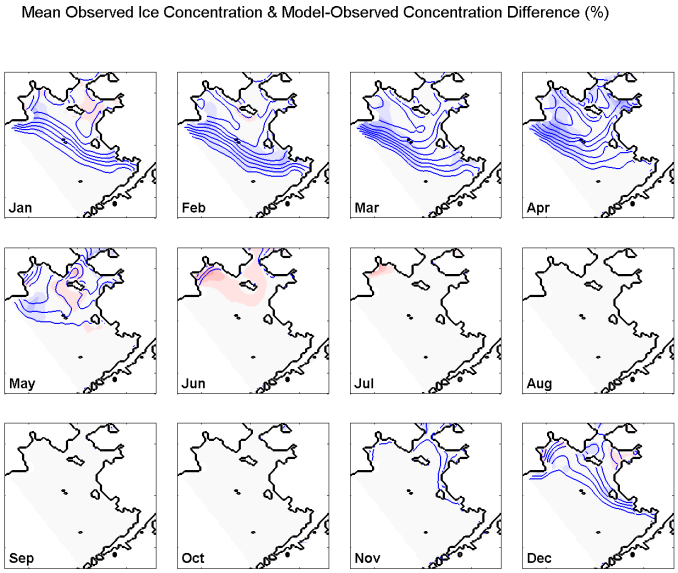

Figure 23: Monthly mean observed and modeled ice concentration differences.

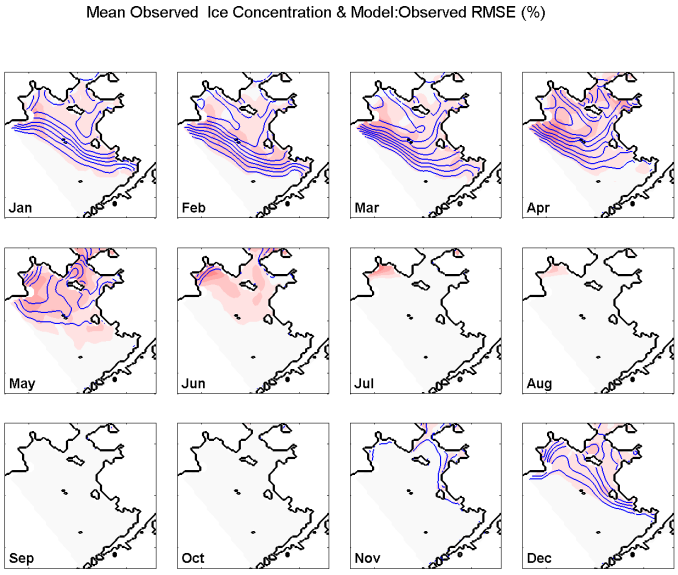

Figure 24: Monthly mean observed and modeled ice concentration root mean squared error.

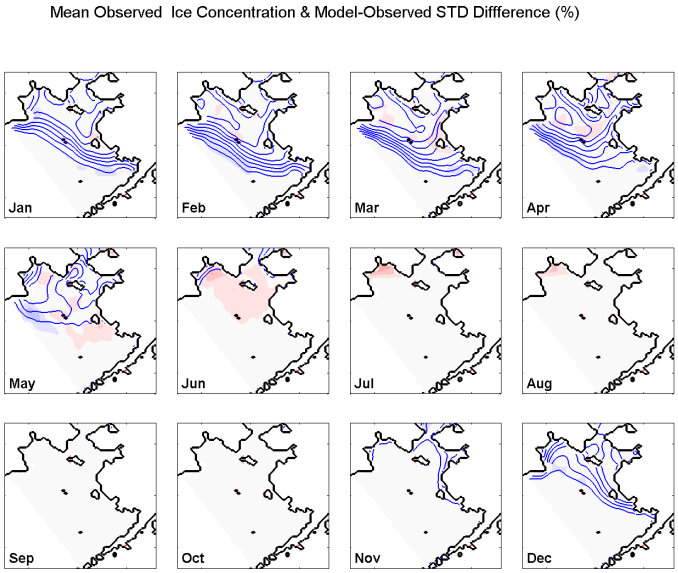

Figure 25: Monthly mean observed and modeled ice concentration standard deviation.

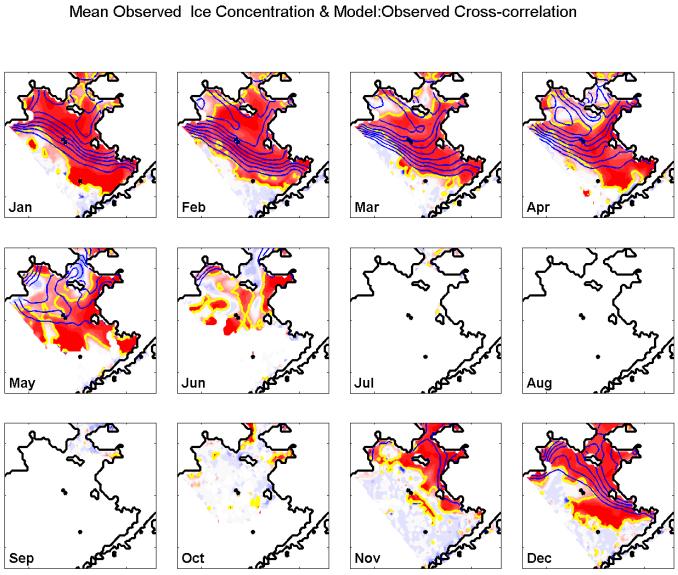

Figure 26: Monthly mean observed and modeled ice concentration cross-correlation.

3.2.4 Transects

Figures 27-32 show model/data comparisons along a transect off Cape Newenham. The difference fields show that the temperature and density offsets seen at mooring M2 extend across the shelf and last through the spring, summer and fall seasons. Positive differences near 25m of depth reflect biases in the model mixed layer depth relative to observations. The mean density and the horizontal gradient panels show that the model generally captures the proper location and magnitude of the two major frontal features (shelf break and nearshore). The offset at the shelf break is likely due to differences between the real and model bathymeteries. Nearshore differences may attributed to the model approximation of river discharge. The vertical density gradient shows that the model exhibits a shallow, strong pycnocline. This feature, like the temperature offset, is linked to the model albedo setting.

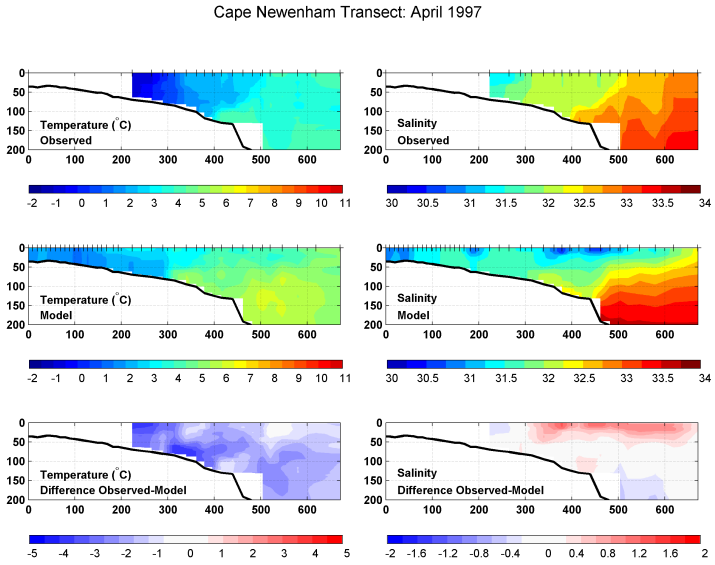

Figure 27: April temperature and salinity observed minus model differences along Cape Newenham transect.

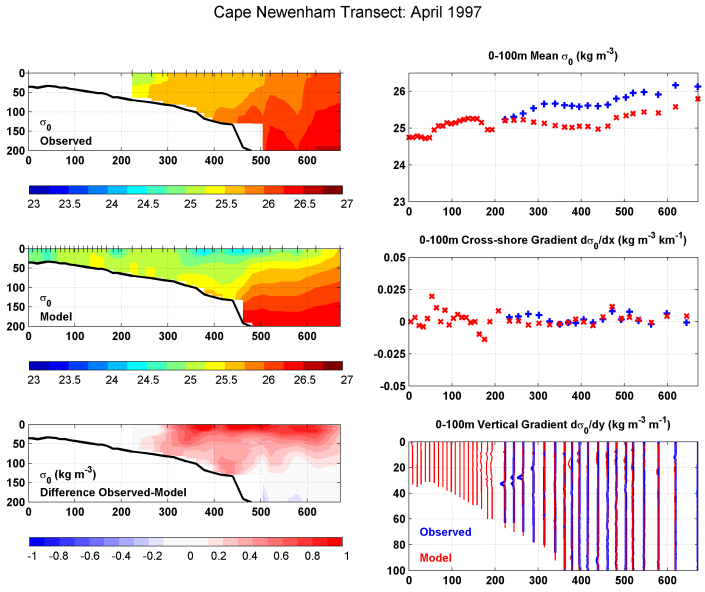

Figure 28: April Density and density gradient comparisons along Cape Newenham transect.

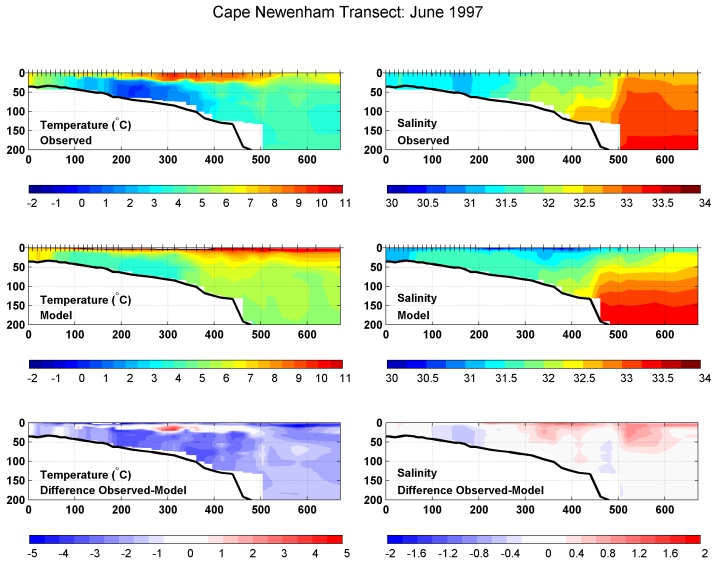

Figure 29: June temperature and salinity observed minus model differences along Cape Newenham transect.

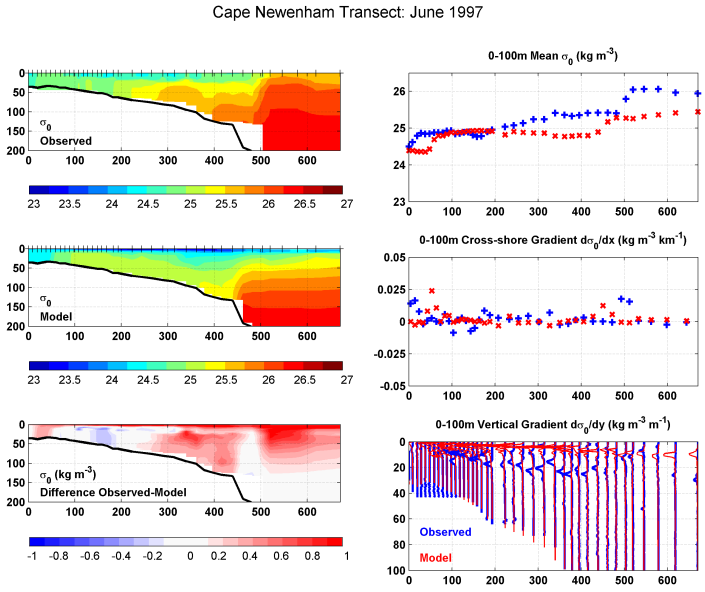

Figure 30: June Density and density gradient comparisons along Cape Newenham transect.

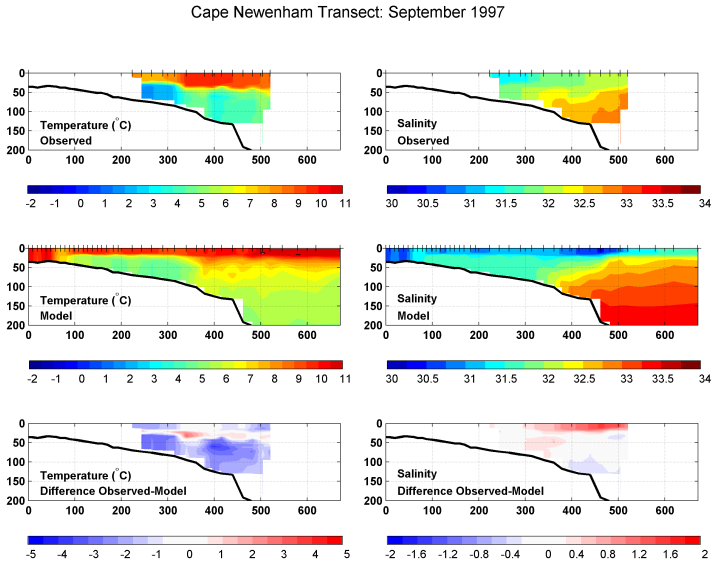

Figure 31: September temperature and salinity observed minus model differences along Cape Newenham transect.

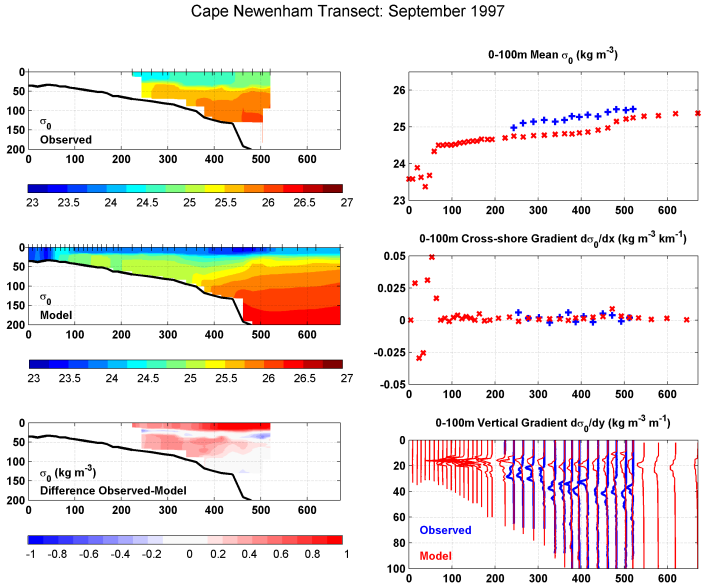

Figure 32: September density and density gradient comparisons along Cape Newenham transect.

3.2.5 Timeseries at M2

The spectra show that in the low frequency band, the model has approximately the right amount of energy (within the 95% confidence bounds) for the near-surface currents. Thus, the current fluctuations at periods between 100 and 1000 hours (4 days to 1.3 months) predicted by the model are statistically similar to those observed at mooring M2. However, at higher frequencies (periods of 10 hours to 100 hours), the model is biased toward the lower 95% limit of the observations, indicating that slightly less kinetic energy is predicted than that observed. The currents found at 50m depth also show no statistically significant difference between the spectra of those predicted and those observed for the 100-1000 hour periods. Likewise, the higher frequency band (10-100 hours) is biased low in the model output at 50 m depth but less so than for the 10 m depth currents. One reason for these low-biased discrepancies might be found in the use of 6-hourly winds to force the ocean surface: 6-hourly winds do not contain the same high frequency spectral content as that observed and the near-surface currents are generally sensitive to wind forcing. This hypothesis is supported by the lack of a distinct inertial peak in the near-surface model CW spectrum. Alternately, it is possible that the model damps the higher frequency motions more strongly than low-frequency motions; the degree of frictional seabed coupling could be partly responsible. Similarly, differences in nonlinear current generation due to turbulence could also partly account for disparity between the observed and modeled currents.

Near the long-term NOAA mooring M2 located in 70m water depth on the Bering Sea shelf, we find that the model captures 40-50% of the monthly temperature variability and 20% of the monthly salinity variability after the mean monthly climatology has been removed

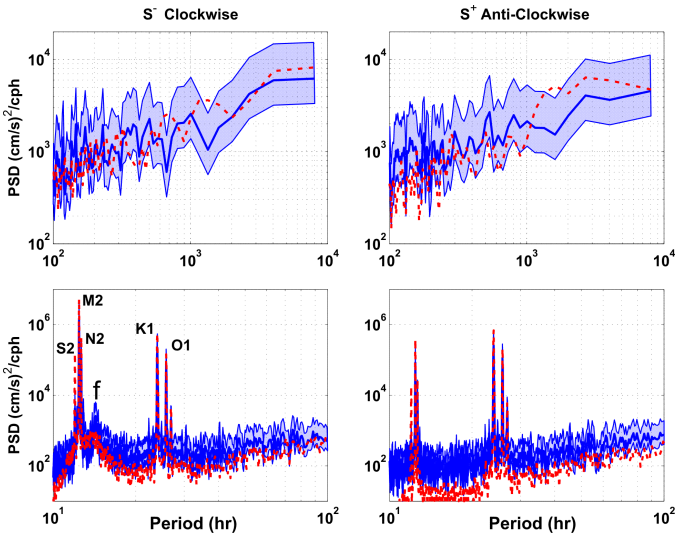

Figure 33: Power spectra at 10 m depth at mooring site M2. Model (red) and observations (blue).

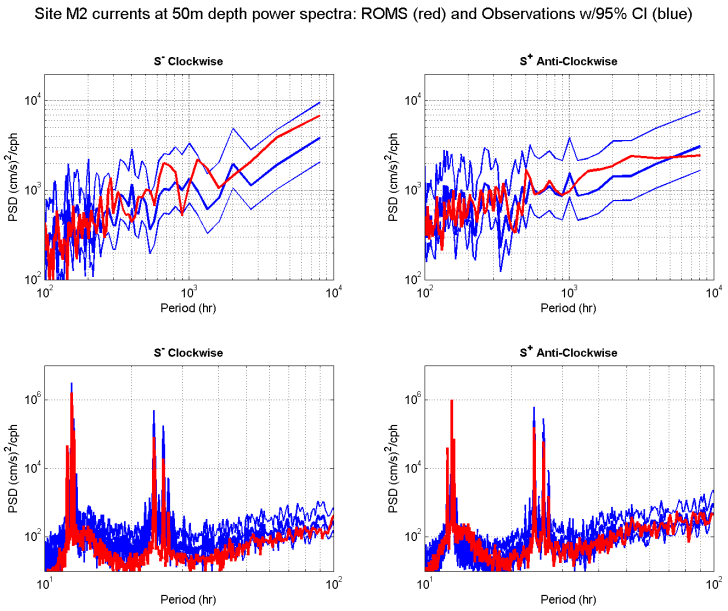

Figure 34: Power spectra at 50 m depth at mooring site M2. Model (red) and observations (blue).

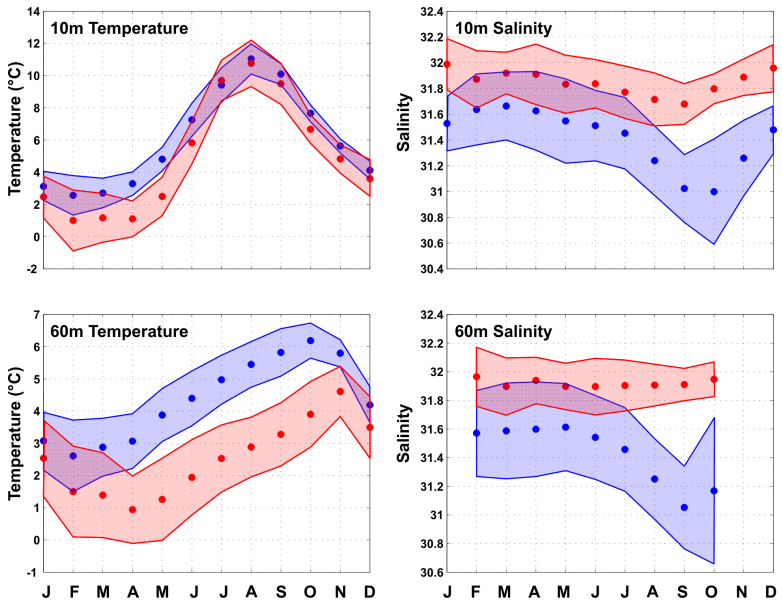

Figure 35: Site M2: Monthly mean and +/-1 standard deviation for temperature and salinity at 10m and 60m. Observations are in red, model in blue.

from the moored T/S records. The simulated T and S fields exhibit mean monthly offsets of -0.3 to +2.6 C and -0.9 to -0.3 PSU respectively. Excluding November, December and January for lack of data, the observed vs. simulated density gradient between the 10 m to 60 m depth levels agrees to within 0.15 kg m-3 in all months except July, August and September where the difference is between 0.3 and 0.4 kg m-3. The model under-estimates the magnitude of this gradient in all months except May.

The following four tables give additional details on the model and data computed statistics:

10m Temperature: 1995 to 2006 Site M2 comparison of monthly data											
	N	Mean		Std Dev		Maximum		Minimum		Corr.	RMSD
		Model	Obs.	Model	Obs.	Model	Obs.	Model	Obs.		
January	9	3.12	2.47	0.86	1.32	4.78	4.35	1.99	0.44	0.90	0.75
February	11	2.56	1.01	1.22	1.89	4.89	3.60	1.17	-1.44	0.90	0.89
March	11	2.71	1.17	0.92	1.52	4.47	3.09	1.22	-1.03	0.75	0.90
April	11	3.29	1.10	0.73	1.12	4.29	2.49	1.98	-1.00	0.43	0.90
May	12	4.81	2.50	0.74	1.20	5.88	4.41	3.48	0.05	0.73	0.79
June	12	7.26	5.83	1.03	1.32	8.87	7.74	5.91	3.83	0.64	0.88
July	11	9.41	9.70	1.06	1.26	11.19	11.51	8.14	8.09	-0.10	1.19
August	11	11.04	10.76	0.94	1.44	12.39	12.58	9.52	8.48	0.49	1.01
September	11	10.09	9.49	0.65	1.28	11.48	11.56	8.92	7.97	0.82	0.83
October	9	7.66	6.67	0.52	0.88	8.32	7.83	6.78	5.74	0.34	0.84
November	9	5.63	4.83	0.44	0.88	6.17	6.22	4.86	3.56	0.72	0.74
December	9	4.12	3.60	0.56	1.09	5.01	5.39	3.21	2.35	0.83	0.74
Mean	11	5.98	4.93	0.81	1.27	7.31	6.73	4.77	3.09	0.62	0.87

Table 1: Temperature statistics at 10m for model and data

60m Temperature: 1995 to 2006 Site M2 comparison of monthly data											
	N	Mean		Std Dev		Maximum		Minimum		Corr.	RMSD
		Model	Obs.	Model	Obs.	Model	Obs.	Model	Obs.		
January	7	3.08	2.54	0.91	1.19	4.79	4.35	1.99	1.00	0.86	0.67
February	8	2.61	1.50	1.11	1.41	4.88	3.47	1.51	-0.50	0.84	0.77
March	8	2.88	1.39	0.90	1.32	4.47	3.05	1.77	-0.44	0.64	0.86
April	10	3.07	0.94	0.85	1.05	4.29	2.34	1.67	-0.75	0.50	0.85
May	10	3.88	1.26	0.82	1.27	5.36	3.10	2.57	-0.59	0.60	0.89
June	10	4.40	1.94	0.85	1.17	5.73	3.44	3.12	0.21	0.81	0.68
July	10	4.97	2.53	0.76	1.04	6.02	3.71	3.60	0.99	0.81	0.67
August	10	5.45	2.88	0.71	0.93	6.33	3.92	3.98	1.52	0.84	0.60
October	9	6.19	3.90	0.54	1.02	7.30	6.13	5.26	2.22	0.95	0.60
November	7	5.80	4.61	0.42	0.78	6.31	5.54	5.16	3.56	-0.06	0.83
December	7	4.19	3.50	0.55	0.95	5.02	4.75	3.33	2.37	0.86	0.63
Mean	9	4.36	2.52	0.76	1.09	5.58	4.07	3.19	0.96	0.70	0.73

Table 2: Temperature statistics at 60m for model and data

10m Salinity: 1995 to 2006 Site M2 comparison of monthly data											
	N	Mean		Std Dev		Maximum		Minimum		Corr.	RMSD
		Model	Obs.	Model	Obs.	Model	Obs.	Model	Obs.		
January	9	31.53	31.99	0.21	0.20	31.80	32.23	31.15	31.69	0.58	0.39
February	11	31.64	31.87	0.28	0.22	32.01	32.22	31.09	31.53	0.46	0.44
March	11	31.66	31.92	0.26	0.16	32.07	32.14	31.27	31.62	0.24	0.46
April	11	31.63	31.91	0.30	0.23	32.10	32.12	31.01	31.27	0.61	0.43
May	12	31.55	31.83	0.33	0.23	31.95	32.11	31.01	31.28	0.48	0.50
June	12	31.51	31.84	0.27	0.19	31.97	32.15	31.07	31.41	0.52	0.44
July	11	31.45	31.77	0.28	0.20	31.93	32.02	31.00	31.28	0.48	0.43
August	11	31.24	31.72	0.27	0.21	31.80	32.01	30.86	31.24	0.58	0.42
September	10	31.02	31.68	0.26	0.16	31.35	31.92	30.40	31.37	0.30	0.44
October	9	31.00	31.80	0.41	0.12	31.63	31.99	30.45	31.60	0.35	0.55
November	9	31.26	31.89	0.29	0.14	31.62	32.20	30.63	31.75	0.56	0.40
December	9	31.48	31.96	0.19	0.18	31.75	32.33	31.13	31.74	0.39	0.38
Mean	10	31.41	31.85	0.28	0.19	31.83	32.12	30.92	31.48	0.46	0.44

Table 3: Salinity statistics at 10m for model and data

60m Salinity: 1995 to 2006 Site M2 comparison of monthly data											
	N	Mean		Std Dev		Maximum		Minimum		Corr.	RMSD
		Model	Obs.	Model	Obs.	Model	Obs.	Model	Obs.		
January	0										
February	4	31.57	31.96	0.30	0.21	32.01	32.17	31.34	31.70	0.83	0.36
March	4	31.59	31.90	0.33	0.20	32.07	32.11	31.33	31.67	0.60	0.43
April	9	31.60	31.94	0.33	0.16	32.10	32.09	31.01	31.60	0.55	0.48
May	10	31.61	31.90	0.30	0.16	31.95	32.08	31.19	31.53	0.45	0.46
June	10	31.54	31.90	0.29	0.20	31.97	32.15	31.07	31.45	0.40	0.46
July	10	31.46	31.90	0.29	0.18	31.93	32.11	31.00	31.51	0.37	0.46
August	10	31.25	31.91	0.28	0.15	31.80	32.08	30.86	31.63	0.37	0.43
September	10	31.05	31.91	0.29	0.11	31.41	32.08	30.40	31.72	0.55	0.43
October	3	31.17	31.95	0.51	0.12	31.63	32.07	30.62	31.83	-0.66	0.67
November	0										
December	0										
Mean	8	31.43	31.92	0.32	0.17	31.87	32.10	30.98	31.63	0.38	0.46

Table 4: Salinity statistics at 60m for model and data

The time series plots (figures 36-38) show the temporal distribution of moored temperature and salinity data. Data collection began in 1995 and continues through the present. We observe a net offset between the model and data, with the bias more pronounced at depth. This bias is also seen in the scatter plots (figure 40).

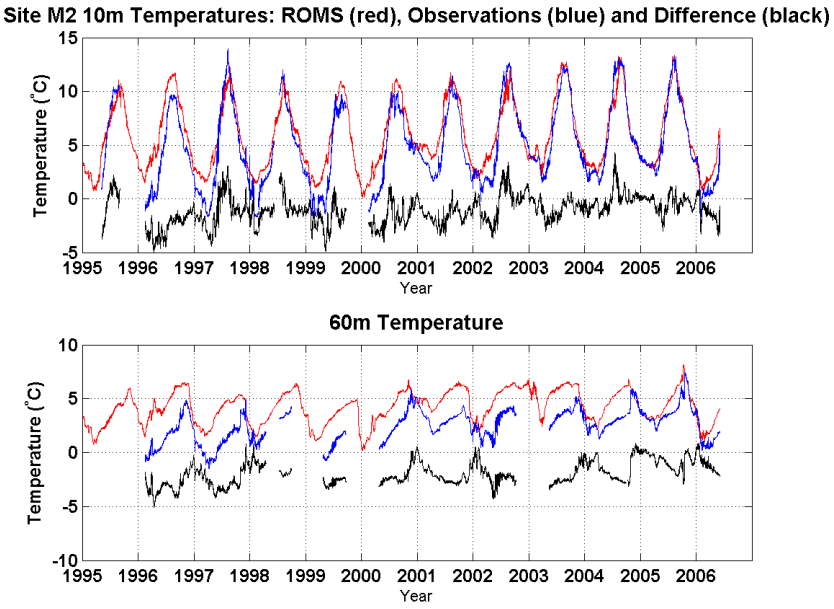

Figure 36: Site M2: Temperature time series comparison at 10m and 60m.

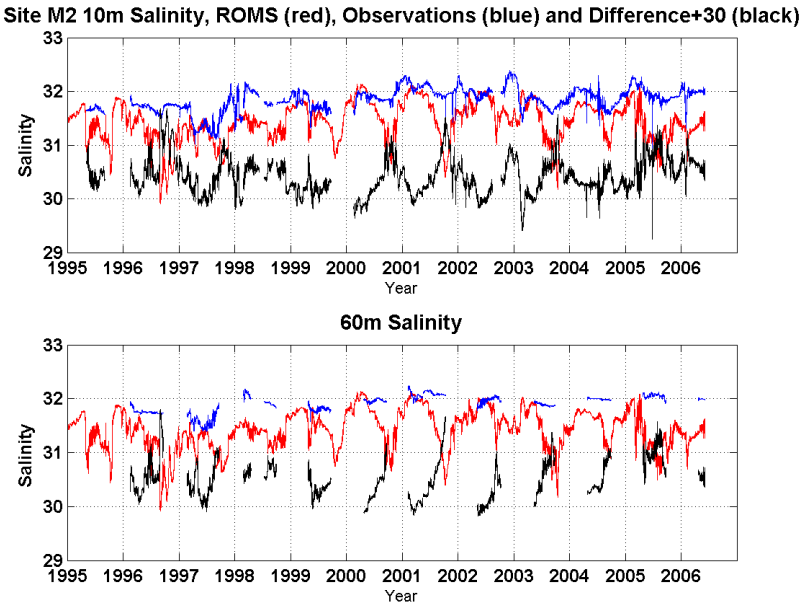

Figure 37: Site M2: Salinity time series comparison at 10m and 60m.

3.2.6 Shelf-wide T and S

Point-to-point evaluations are often difficult for a model since it is not expected that a model reproduce turbulent variability precisely as in nature. Therefore a planar view can be instructive for overall model performance. Figures 41-48 compare model temperature and salinity for the Bering shelf and show that the model reproduces with appreciable skill the structure and variability of these fields. In these figures, the model results and observational data have been re-gridded to an identical mesh so that direct comparisons can be made between the two. In all cases, the color scales are the same for the two output fields and the spatial mean has been subtracted everywhere to eliminate the bias of constant offsets.

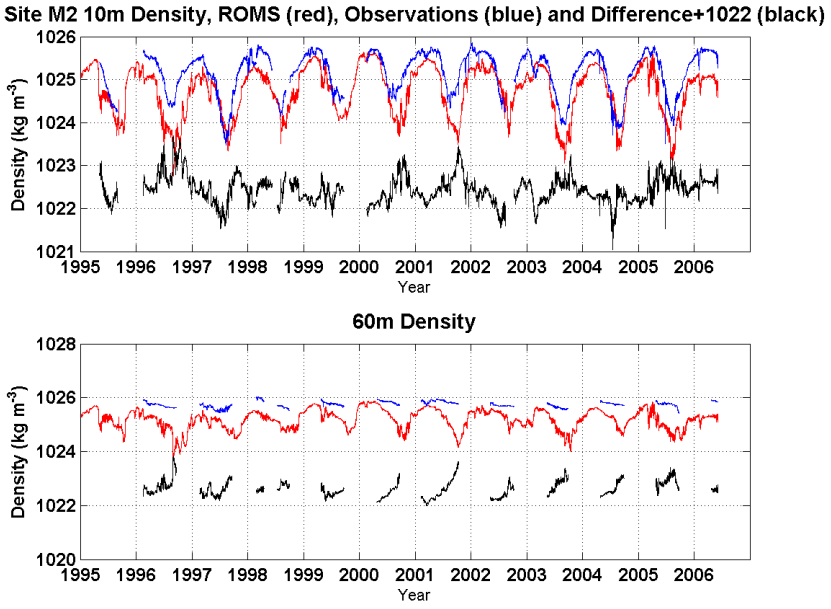

Figure 38: Site M2: Timeseries of density at 10m and 60m.

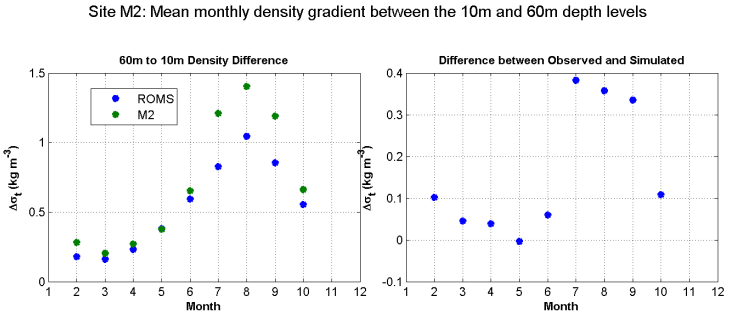

Figure 39: Site M2: Monthly mean density gradient (60 to 10m).

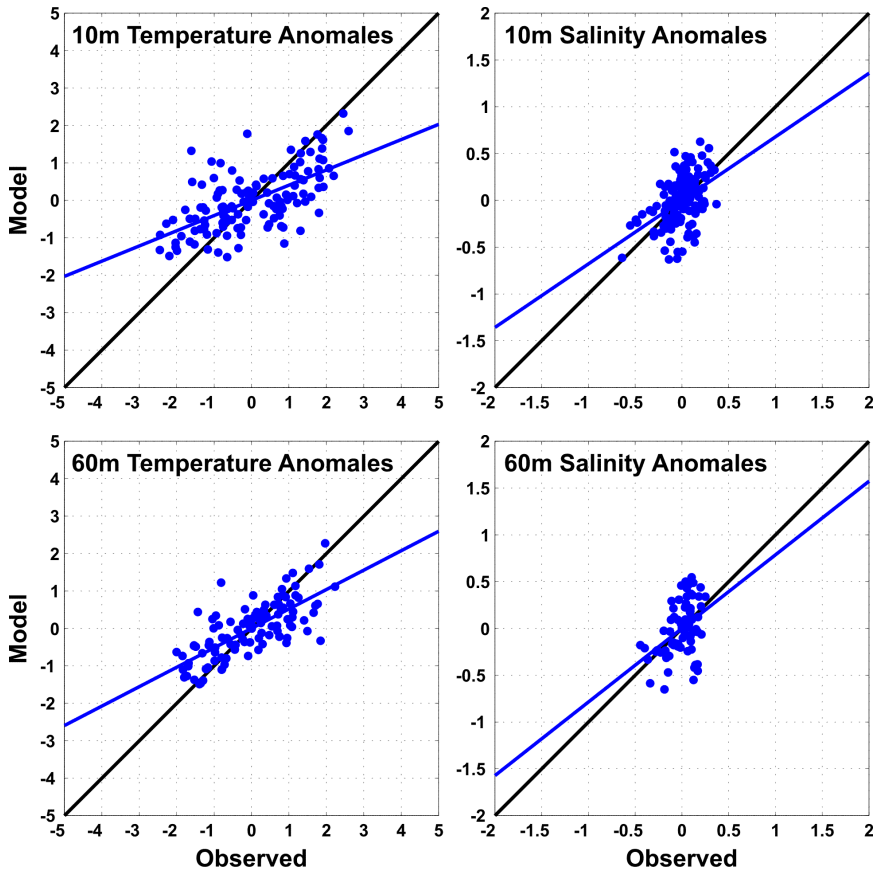

Figure 40: Site M2: Monthly mean temperature and salinity scatter plots for 10m and 60m

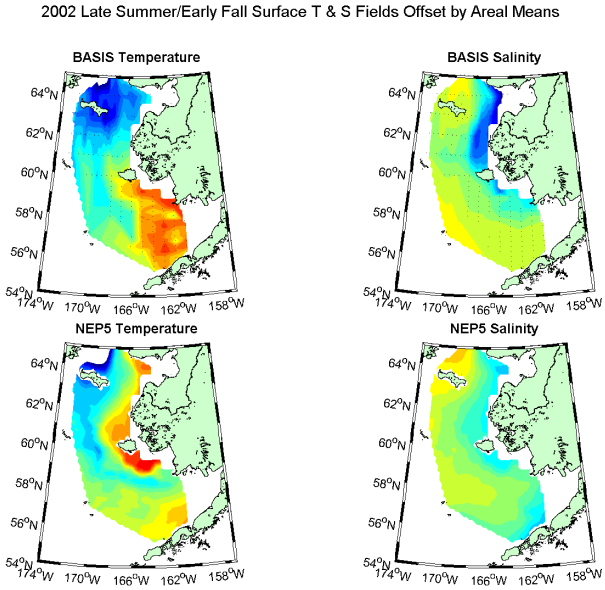

Figure 41: Model vs. BASIS surface temperature and salinity comparisons for 2002.

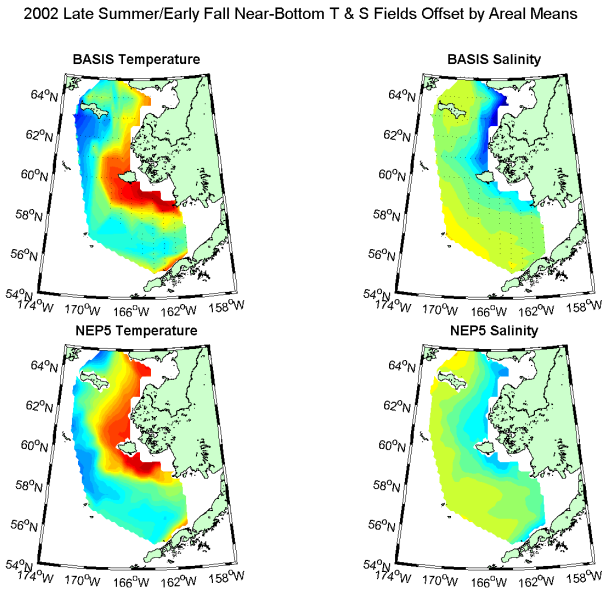

Figure 42: Model vs. BASIS near bottom temperature and salinity comparisons for 2002.

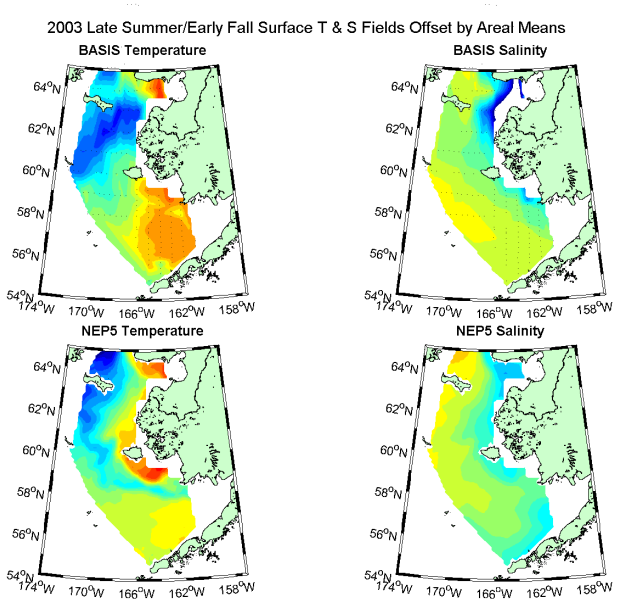

Figure 43: Model vs. BASIS surface temperature and salinity comparisons for 2003.

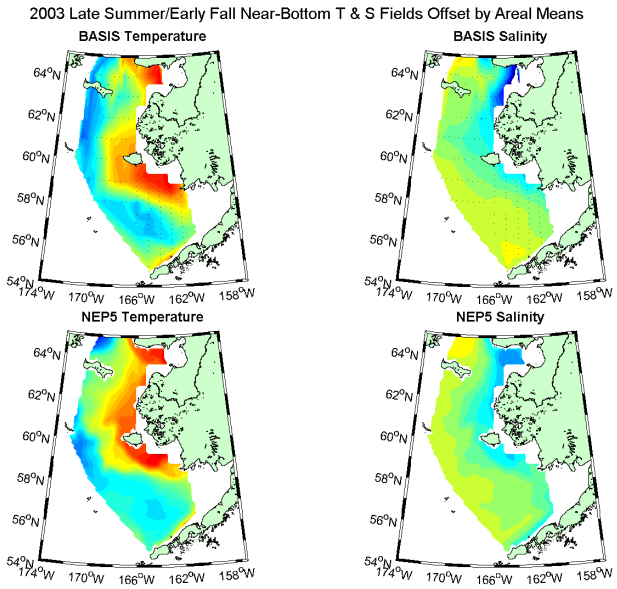

Figure 44: Model vs. BASIS near bottom temperature and salinity comparisons for 2003.

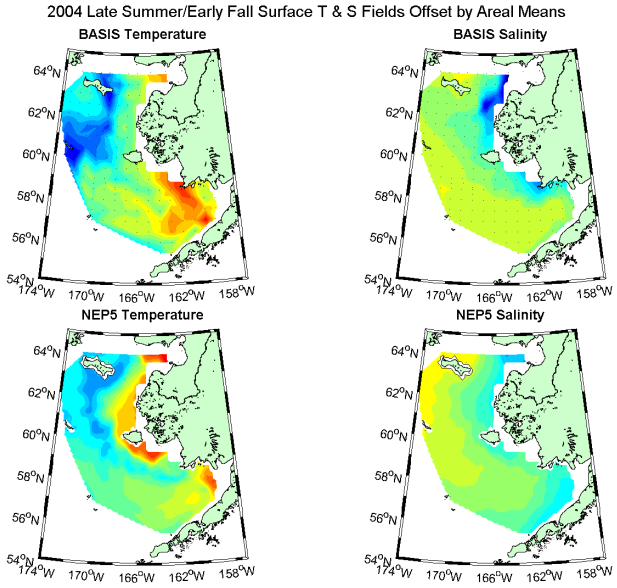

Figure 45: Model vs. BASIS surface temperature and salinity comparisons for 2004.

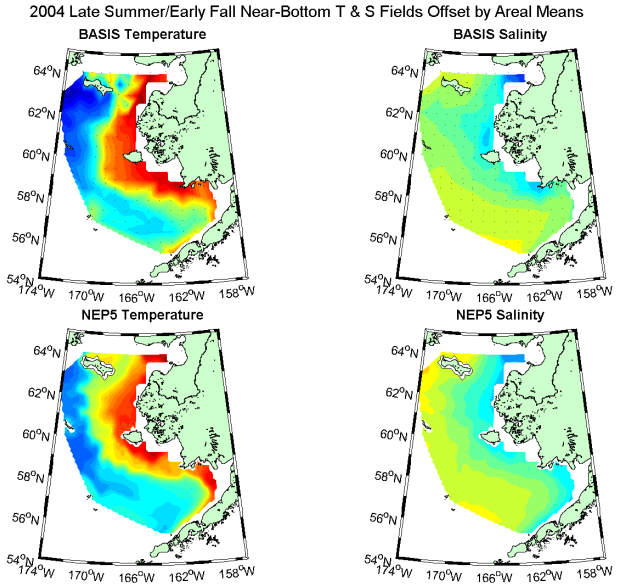

Figure 46: Model vs. BASIS near bottom temperature and salinity comparisons for 2004.

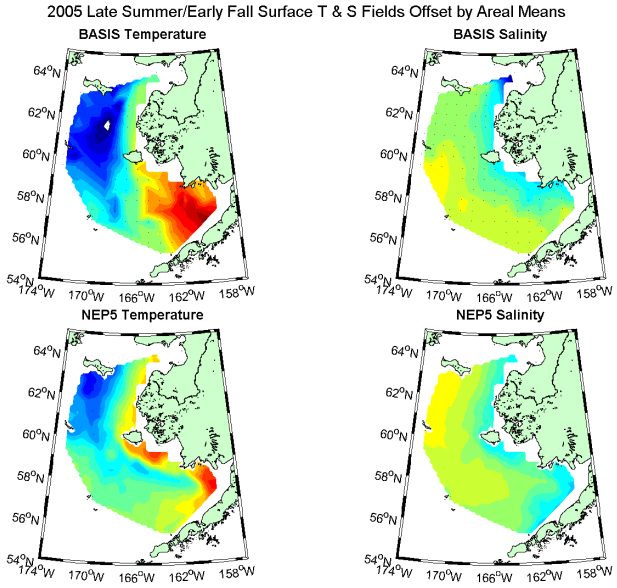

Figure 47: Model vs. BASIS surface temperature and salinity comparisons for 2005.

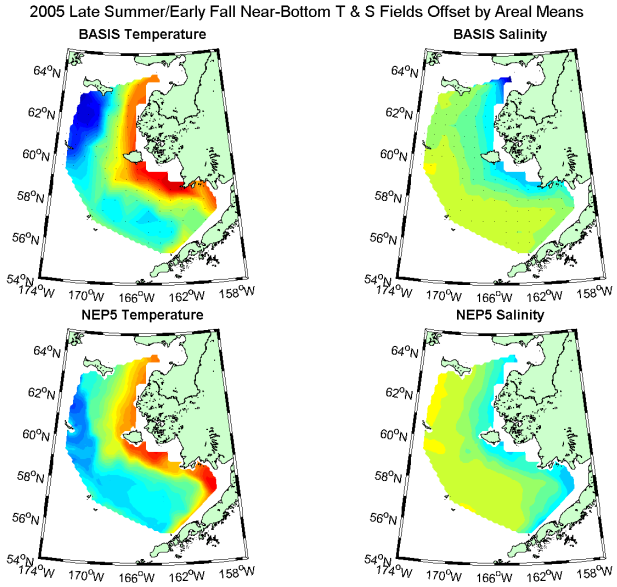

Figure 48: Model vs. BASIS near bottom temperature and salinity comparisons for 2005.

4 Summary remarks

We presented results from a regional coupled circulation-sea ice model of the Bering Sea which was run in hindcast mode for the 1985-2005 period. A significant effort was spent on model evaluation. Though the focus of the study was on the North Aleutian Basin (NAB), in order to achieve a more comprehensive evaluation of model performance datasets in the Bering Sea beyond the NAB were also used. The data we used was a combination of multi-year timeseries from moorings, drifter data, satellite and ship transect data.

As a general statement, the model exhibits predictive skill in this region. However, the skill is not uniform in all variables or on all scales. Sea ice cover is generally well represented in the model. Model kinetic energy is similar to observations at frequencies lower than three days and at tidal frequencies, but the inertial peak is missing in the model and the noise floor between 10 and 100 hours is biased low. We speculate that this is primarily due to the wind forcing dataset which itself does not resolve the inertial frequency. The seasonal and interannual temperature and salinity variability in the model matches well with time series observations at NOAA mooring M2. A comparison with transect data shows the model reproduces the seasonal transitions in the water column from a well-mixed shelf regime, to a highly-stratified two-layer system during the summer at the mid-shelf, although the depth and strength of stratification are still difficult parameters to resolve. The near-shore remains well mixed throughout the year both in the data and the model results; energy for mixing is supplied from both wind and tide forcing. Particular care was taken in the implementation of the tides in this model. We deemed this to be important because tides are known to represent a significant amount of the total kinetic energy of the system. As a whole, tidal

amplitudes and phases are well represented in the model. However, in particular places where coastal geometry is significant (e.g, Cook Inlet) the model does exhibit errors.

References

[1] Budgell, W.P, 2005. Numerical simulation of ice-ocean variability in the Barents Sea region: Towards dynamical downscaling. Ocean Dyn. 55: 370-387.

[2] Carton JA, Chepurin G, Cao X (2000a) A simple ocean data assimilation analysis of the global upper ocean 1950-1995, part 2: results. J Phys Oceanogr 30:311326.

[3] Carton JA, Chepurin G, Cao X, Giese B (2000b) A simple ocean data assimilation analysis of the global upper ocean 1950-1995, part 1: methodology. J Phys Oceanogr 30:294309.

[4] Coachman, L. K., 1982. Flow convergence over a broad, flat continental shelf. Cont. Shelf Res., 1, 1-14.

[5] Coachman, L. K., 1986. Circulation, water masses and fluxes on the southeastern Bering Sea shelf. Cont. Shelf Res., 5, 23-108.

[6] Curchitser, E. N., D. B. Haidvogel, A. J. Hermann, E. L. Dobbins, T. M. Powell and A. Kaplan , 2005. Multi-scale modeling of the North Pacific Ocean: Assessment and analysis of simulated basin-scale variability (1996-2003). J. Geophys. Res., 110, C11021, doi:101029/2005JC002902

[7] Danielson, S., K. Aagaard, T. Weingartner, S. Martin, P. Winsor, G. Gawarkiewicz, and D. Quadfasel, 2006. The St. Lawrence polynya and the Bering shelf circulation: New observations and a model comparison, J. Geophys. Res., J111, C09023, doi:10.1029/2005JC003268.

[8] Danielson, S., and Z. Kowalik, 2005. Tidal currents in the St. Lawrence Island region, J. Gephys. Res., 110, No. C10, C10004, 10.1029/2004JC002463.

[9] Egbert, G.D. and S.Y. Erofeeva, 2002. Efficient inverse modeling of barotroptic ocean tides. J. Atmo. Oce. Tech., 19, 183-204.

[10] Fairall, C.W., E.F. Bradley, D.P. Rogers, J.B. Edson and G.S. Young, 1996. Bulk parameterization of air-sea fluxes for tropical ocean-global atmosphere Coupled-Ocean Atmosphere Response Experiment, J. Geophys. Res., 101, 3747-3764.

[11] Hedstrom, K. S., 2010. Technical Manual for a Coupled Sea-Ice/Ocean Circulation Model, Minerals Management Service Report MMS 2009-062.

[12] Hermann, A. J., P. J. Stabeno, D. B. Haidvogel and D. L. Musgrave, 2002. A regional tidal/subtidal circulation model of the southeastern Bering Sea: Development, sensitivity analyses and hindcasting. Deep-Sea Res. II, 49: 5495-5967.

[13] Hermann, A.J., E.N. Curchitser, E.L. Dobbins and D.B. Haidvogel, 2007. A comparison of remote versus local influence of El Nio on the coastal circulation of the Northeast Pacific. Prog. Oceanog., sub. judice.

[14] Huang, H.P., A. Kaplan, E.N. Curchitser, and N. Maximenko, 2007. The degree of anisotropy for mid-ocean currents from satellite observations and an eddy-permitting model simulation. J. Geophys. Res., In press.

[15] Hunke E., 2001. Viscous-plastic sea ice dynamics with the EVP model: Linearization issues. J. Comp. Phys. 170: 1838.

[16] Hunke E. and Dukowicz, J., 1997. An elastic-viscous-plastic model for sea ice dynamics. J. Phys. Oceanogr. 27: 1849-1867.

[17] Kachel, N.B., G.L. Hunt, Jr., S.A. Salo, J.D. Schumacher, P.J. Stabeno, and T.E. Whitledge, 2002: Characteristics and variability of the inner front of the southeastern Bering Sea, Deep-Sea Res. Part II, 49, 5889-5910.

[18] Large, W.G. and Yeager, 2004. Diurnal to decadal global forcing for ocean and Sea-Ice models: The data sets and flux climatologies. NCAR Tech. Note 460.

[19] Large, W. G., J. C. McWilliams and S. C. Doney, 1994. Oceanic vertical mixing: A review and a model with a nonlocal boundary layer parameterization, Rev. Geophysics, 29, 363-403.

[20] Marchesiello, P., J.C. McWilliams, and A. Shchepetkin, 2001: Open boundary conditions for long-term integration of regional ocean models. Ocean Modelling 3, 1-20.

[21] Mellor, G.L. and Kantha, L., 1989. An ice-ocean coupled model. J. Geophys. Res. 94: 10937-10954.

[22] Moore, A. M., H. G. Arango, E. DiLorenzo, B. D. Cornuelle, A. J. Miller, and D. J. Neilsen. 2004. A comprehensive ocean prediction and analysis system based on the tangent linear and adjoint of a regional ocean model, Ocean Modeling, 7, 227.

[23] Roach, A. T., Aagaard, K., Pease, C. H., Salo, S. A., Weingartner, T., Pavlov, V., Kulakov, M., 1995. Direct measurements of transport and water properties through the Bering Strait. J. Geophys. Res., 100: 18443-18457.

[24] Royer, T. C., 1998. Coastal processes in the northern North Pacific, in The Sea, edited by A. R. Robinson and K. H. Brink, pp. 395-414, John Wiley and Sons, New York, NY.

[25] Schumacher, J. D., and R. K. Reed. 1992. Characteristics of currents over the continental slope of the eastern Bering Sea. J. Geophys. Res., 97, 9423-9433.

[26] Schumacher, J. D., and P. J. Stabeno. 1994. Ubiquitous eddies of the eastern Bering Sea basin and their coincidence with concentrations of larval pollock. Fish. Oceanogr., 3, 182-190.

[27] Schumacher, J.D., N.A. Bond, R.D. Brodeur, P.A. Livingston, J.M. Napp, and P.J. Stabeno (2003): Climate change in the Southeastern Bering Sea and some consequences for biota. Chapter 2 in Large Marine Ecosystems of the World: Trends in Exploitation, Protection, and Research, G. Hempel and K. Sherman (eds.), Elsevier Science, Amsterdam, 1740.

[28] Shchepetkin, A. F. and J. C. McWilliams, 1998. Quasi-monotone advection schemes based on explicit locally adaptive dissipation. Mon. Weather Rev., 126, 15411580.

[29] Shchepetkin, A. F., and J. C. McWilliams (2003), A method for computing horizontal pressure-gradient force in an oceanic model with a nonaligned vertical coordinate, J. Geophys. Res., 108(C3), 3090, doi:10.1029/2001JC001047.

[30] Shchepetkin, A. F., and J. C. McWilliams (2005), The Regional Ocean Modeling System: A split explicit, free-surface, topography following coordinates ocean model, Ocean Modelling, 9, 347 404.

[31] Stabeno, P. J. and R. K. Reed. 1994. Circulation in the Bering Sea observed by satellite-tracked drifters: 1986-1993. J. Phys. Oceanogr., 24: 848-854.

[32] Stabeno, P. and P. van Meurs. 1999. Evidence for episodic on-shelf flow. J. Geophys. Res., 104: 29715 - 29720.

[33] Stabeno, P. J., J. D. Schumacher, and K. Ohtani. 1999. The physical oceanography of the Bering Sea. In Dynamics of the Bering Sea: A Summary of Physical, Chemical, and Biological Characteristics, and a Synopsis of Research on the Bering Sea, eds. T. R. Loughlin and K. Ohtani, University of Alaska Sea Grant, AK-SG-99-03, North Pacific Marine Science Organization (PICES), 128.

[34] Steele, M., G.L. Mellor and M.G. McPhee, 1989. Role of the Molecular Sublayer in the Melting or Freezing of Sea Ice, J. Phys. Oceanogr., 19, 139-147.

[35] Yeager, S.G. and W.G. Large, 2004. Late-Winter Generation of Spiciness on Subducted Isopycnals. J. Phys. Oce. 34, pp. 1528-1547.

The Department of the Interior Mission:
Protecting America's Great Outdoors and Powering Our Future
The U.S. Department of the Interior protects America's natural resources and heritage, honors our cultures and tribal communities, and supplies the energy to power our future.